© 2014. Published by The Company of Biologists Ltd | Journal of Cell Science (2014) 127, 2040–2052 doi:10.1242/jcs.143602

RESEARCH ARTICLE

Maintenance of stereocilia and apical junctional complexes by Cdc42 in cochlear hair cells

Takehiko Ueyama[1,*,‡], Hirofumi Sakaguchi[2,*], Takashi Nakamura[1,2], Akihiro Goto[3], Shigefumi Morioka[1,2], Aya Shimizu[1], Kazuki Nakao[4], Yoshitaka Hishikawa[5], Yuzuru Ninoyu[1,2], Hidetoshi Kassai[4], Shiro Suetsugu[6], Takehiko Koji[7], Bernd Fritzsch[8], Shigenobu Yonemura[9], Yasuo Hisa[2], Michiyuki Matsuda[3], Atsu Aiba[4] and Naoaki Saito[1,‡]

ABSTRACT

Cdc42 is a key regulator of dynamic actin organization. However, little is known about how Cdc42-dependent actin regulation influences steady-state actin structures in differentiated epithelia. We employed inner ear hair-cell-specific conditional knockout to analyze the role of Cdc42 in hair cells possessing highly elaborate stable actin protrusions (stereocilia). Hair cells of *Atoh1–Cre;Cdc42*$^{flox/flox}$ mice developed normally but progressively degenerated after maturation, resulting in progressive hearing loss particularly at high frequencies. Cochlear hair cell degeneration was more robust in inner hair cells than in outer hair cells, and began as stereocilia fusion and depletion, accompanied by a thinning and waving circumferential actin belt at apical junctional complexes (AJCs). Adenovirus-encoded GFP–Cdc42 expression in hair cells and fluorescence resonance energy transfer (FRET) imaging of hair cells from transgenic mice expressing a Cdc42-FRET biosensor indicated Cdc42 presence and activation at stereociliary membranes and AJCs in cochlear hair cells. *Cdc42*-knockdown in MDCK cells produced phenotypes similar to those of *Cdc42*-deleted hair cells, including abnormal microvilli and disrupted AJCs, and downregulated actin turnover represented by enhanced levels of phosphorylated cofilin. Thus, Cdc42 influenced the maintenance of stable actin structures through elaborate tuning of actin turnover, and maintained function and viability of cochlear hair cells.

KEY WORDS: Cdc42, Deafness, Stereocilia, Hair cell, Apical junctional complex, Actin turnover, FRET

[1]Laboratory of Molecular Pharmacology, Biosignal Research Center, Kobe University, Kobe 657-8501, Japan. [2]Department of Otolaryngology-Head and Neck Surgery, Kyoto Prefectural University of Medicine, Kyoto 602-8566, Japan. [3]Laboratory of Bioimaging and Cell Signaling, Graduate School of Biostudies, Kyoto University, Kyoto 606-8315, Japan. [4]Laboratory of Animal Resources, Center for Disease Biology and Integrative Medicine, Faculty of Medicine, University of Tokyo, Tokyo 113-0033, Japan. [5]Division of Histochemistry and Cell Biology, Department of Anatomy, Faculty of Medicine, University of Miyazaki, Miyazaki 889-1692, Japan. [6]Laboratory of Membrane and Cytoskeleton Dynamics, Institute of Molecular and Cellular Biosciences, Univeristy of Tokyo, Tokyo 113-0032, Japan. [7]Department of Histology and Cell Biology, Nagasaki University Graduate School of Biomedical Sciences, Nagasaki 852-8523, Japan. [8]Department of Biology, College of Liberal Arts and Sciences, University of Iowa, Iowa, IA 52242, USA. [9]Electron Microscope Laboratory, Center for Developmental Biology, RIKEN, Kobe 650-0047, Japan.
*These authors contributed equally to this work

‡Authors for correspondence (tueyama@kobe-u.ac.jp; naosaito@kobe-u.ac.jp)

Received 30 September 2013; Accepted 22 January 2014

INTRODUCTION

Dynamic actin turnover and rearrangement alter overall cell geometry and polarity, as well as local membrane topology, to form distinct cellular structures (Campellone and Welch, 2010). In some structures, such as lamellipodia and the *Listeria* comet tail, actin filaments are highly dynamic with a turnover rate measured in seconds (Ponti et al., 2004; Theriot et al., 1992), whereas they are relatively stable in stereocilia (Schwander et al., 2010) and apical junctional complexes (AJCs) (Ivanov et al., 2005).

Stereocilia and AJCs are present in inner ear hair cells, which are specialized sensory epithelia detecting hearing and balance. In the cochlea, hair cells are arranged in a single row of inner hair cells (IHCs) and three rows of outer hair cells (OHCs). Although IHCs and OHCs are believed to share common mechanotransduction machinery, they have distinct roles during sound detection: IHCs are true sensors, whereas OHCs function as an amplifier through an active process that involves stereociliary and somatic motility (Matsumoto et al., 2010; Schwander et al., 2010). Stereocilia, which are actin-based protrusions, are known as exquisitely organized microvilli and filopodia composed of hundreds of parallel actin filaments with the plus ends at the distal tip; however, stereocilia are organized into precise rows of graded height (Frolenkov et al., 2004). High sensitivity of hair cells depends on the coordinated movement of stereocilia upon mechanical stimulation; thus, the length and shape of stereocilia are determined precisely. Moreover, as hair cells are usually not replaced (Collado et al., 2008), turnover of stereociliary components is a lifetime requirement. Although a recent model has suggested that stereocilia maintain their steady state through treadmill-like dynamic actin turnover (Rzadzinska et al., 2004), others have reported no such finding (Zhang et al., 2012), raising a question about the actin turnover mechanism in stereocilia. AJCs are another actin structure essential for hair cell function, such as the maintenance of a proper cell arrangement and the epithelial barrier (Collado et al., 2011). However, the mode and effect of actin turnover at AJCs remain unknown (Nunes et al., 2006).

Cdc42 is a key regulator of the actin cytoskeleton. However, the function of Cdc42 in hair cells has not been studied, particularly regarding the development and maintenance of stereocilia. Cdc42, Rac1 and RhoA are the best characterized Rho-family small GTPases, and all are expressed in hair cells (Kalinec et al., 2000). Although they have common regulators and effectors, their activity results in different effects. Cdc42 is essential for filopodia formation (Chen et al., 2000; Yang et al., 2006), whereas Rac and RhoA induce lamellipodia and stress

Journal of Cell Science

Journal of Cell Science (2014) 127, 2040–2052 doi:10.1242/jcs.143602

fiber formation, respectively (Heasman and Ridley, 2008). Cdc42 induces actin polymerization through its interaction with actin nucleators (Campellone and Welch, 2010), including the Arp2/3 complex component N-WASP (Takenawa and Suetsugu, 2007), and promotes filopodia induction and stabilization through the PAK/LIM kinase (LIMK) pathway and the cofilin phosphorylation cycle (Matsumoto et al., 2010; Melendez et al., 2011). Cdc42 also regulates AJC formation *in vitro* (Otani et al., 2006; Qin et al., 2010) and *in vivo* (Melendez et al., 2011).

Here, we show that Cdc42 is localized and it functions at stereociliary membranes and AJCs for their maintenance in hair cells. *Cdc42* deletion resulted in abnormal stereocilia and AJC morphology, and was associated with downregulated actin turnover, leading to slowly progressive cochlear hair cell loss. These data provide new insights into the function of Cdc42 at apical protrusions and AJCs in differentiated epithelia *in vivo*.

RESULTS

Inactivation of the *Cdc42* gene in inner ear hair cells by use of *Atoh1–Cre* transgenic mice

We examined and confirmed expression of *Cdc42* mRNA in cochlea using a reverse transcription polymerase chain reaction (RT-PCR; data not shown) and *in situ* hybridization (ISH) (Fig. 1A). We used the *Atoh1* promoter, a basic helix-loop-helix (bHLH) transcription factor for hair-cell-specific inactivation of *Cdc42* (Chen et al., 2002; Jahan et al., 2013). The pattern of *Atoh1–Cre*-directed recombination was assessed in the inner ear at embryonic day (E) 13.5 and E15.5 as well as postnatal day 3 (P3) by assessing the β-galactosidase activity of rearranged *CAG-*^{flox}*CAT*^{flox}*-LacZ* reporter mice (hereafter referred to as *Atoh1–Cre;LacZ*). Consistent with a previous report (Chen et al., 2002), X-gal staining was first observed at E15.5 in the cochlea and vestibule of *Atoh1–Cre;LacZ* mice but not in control (*CAG-*^{flox}*CAT*^{flox}*-LacZ*) mice (data not shown). Cochlear X-gal staining was restricted to IHCs and OHCs at P3 (supplementary material Fig. S1A). Immunostaining against Cre also showed a specific signal in IHCs and OHCs at P1 of *Atoh1–Cre*$^{+/-}$ mice but not in littermate *Atoh1–Cre*$^{-/-}$ mice (supplementary material Fig. S1B). We attempted to detect endogenous Cdc42 using two different anti-Cdc42 antibodies but could not detect a specific signal in inner ear tissues with conventional fixation. Therefore, we used trichloroacetic acid (TCA) fixation, known to be effective for several antibodies against actin-related proteins (Hayashi et al., 1999). Cdc42 immunoreactivity was detected in TCA-fixed IHCs and OHCs at P0, with particularly intense reactivity in stereocilia of *Cdc42*$^{flox/flox}$ mice (Fig. 1B), which was consistent with a report stating that Cdc42 is a hair bundle (stereocilia) protein (Shin et al., 2013). As expected, this reactivity was absent in the hair cells of *Atoh1–Cre;Cdc42*$^{flox/flox}$ mice (Fig. 1B).

Progressive hearing loss and cochlear hair cell loss in *Atoh1–Cre;Cdc42*$^{flox/flox}$ mice

In order to assess cochlear function, we first used auditory brainstem response (ABR), an electrophysiological hearing test that detects evoked potentials in the auditory pathway from the cochlea to the upper brainstem. We examined hearing in 2–8-week-old *Atoh1–Cre;Cdc42*$^{flox/flox}$ mice using ABR with broadband click stimuli corresponding to the low frequencies at 2–4 kHz (Fig. 2A). No differences were observed in hearing between age-matched *Cdc42*$^{flox/flox}$ mice and *Atoh1–Cre;Cdc42*$^{+/+}$ mice at 3 weeks or heterozygous *Atoh1–Cre;Cdc42*$^{flox/+}$ mice at 8

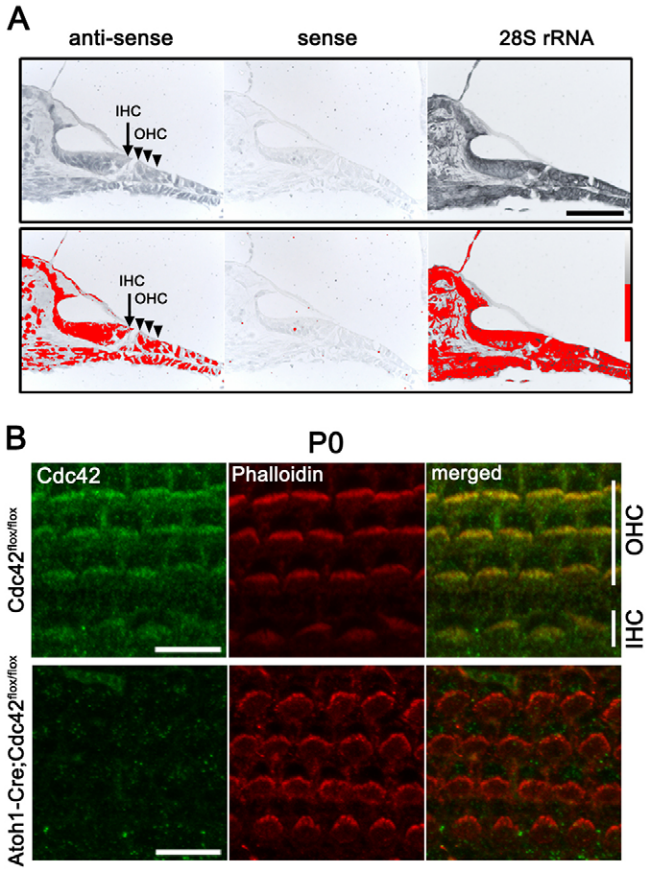

Fig. 1. *Cdc42*-mRNA expression in cochlea and Cdc42 localization at cochlear stereocilia. (A) *In situ* hybridization (upper panel) detects *Cdc42* mRNA expression in cochlear inner hair cell (IHC, arrow) and outer hair cell (OHC; arrowheads) of P5 wild-type mice. The lower panel shows the relative *Cdc42* mRNA signal level determined by the DAB image analyzer (red was assigned to positive). A *28S* rRNA complementary oligo-DNA probe was used as a positive control. Scale bar: 50 µm. (B) Cdc42 (green) and filamentous actin (red) immunostaining in TCA-fixed organs of Corti from *Cdc42*$^{flox/flox}$ and *Atoh1–Cre;Cdc42*$^{flox/flox}$ mice at P0. Note the absence of Cdc42 staining in stereocilia of *Atoh1–Cre;Cdc42*$^{flox/flox}$ mice. Scale bars: 10 µm.

weeks [$n \geq 6$; 20.0±3.2 versus 18.3±2.8 dB sound pressure level (SPL); $n \geq 6$; 21.7±4.8 versus 25.0±4.9 dB SPL, respectively]; *Cdc42*$^{flox/flox}$ mice were used as controls for all subsequent studies. At 2 weeks, *Atoh1–Cre;Cdc42*$^{flox/flox}$ mice had a slightly elevated ABR threshold compared with that in control mice (Fig. 2A, 35.0±2.3 versus 23.1±2.2 dB SPL), progressing to 70.5±3.2 dB SPL by 8 weeks (Fig. 2A). An 8–32 kHz tone-burst stimulation resulted in severe hearing loss particularly at high frequencies from 2 weeks (Fig. 2B). We further confirmed hearing loss in *Atoh1–Cre;Cdc42*$^{flox/flox}$ mice using the distortion product otoacoustic emission (DPOAE) response, which detects a low-level sound generated by the active mechanism of OHCs that is emitted to the ear canal. A significant decrease in the DPOAE level was detected at 4 weeks in response to high frequencies and progressively deteriorated to encompass all frequencies by 8 weeks (Fig. 2C). Although *Atoh1* also functions in vestibular hair cells (Chen et al., 2002), *Atoh1–Cre;Cdc42*$^{flox/flox}$ mice had no detectable balance impairment and exhibited normal gait and swimming ability throughout their lives.

No obvious changes in gross tissue morphology were detected in either the cochlea or the vestibule, including the sensory

Journal of Cell Science (2014) 127, 2040–2052 doi:10.1242/jcs.143602

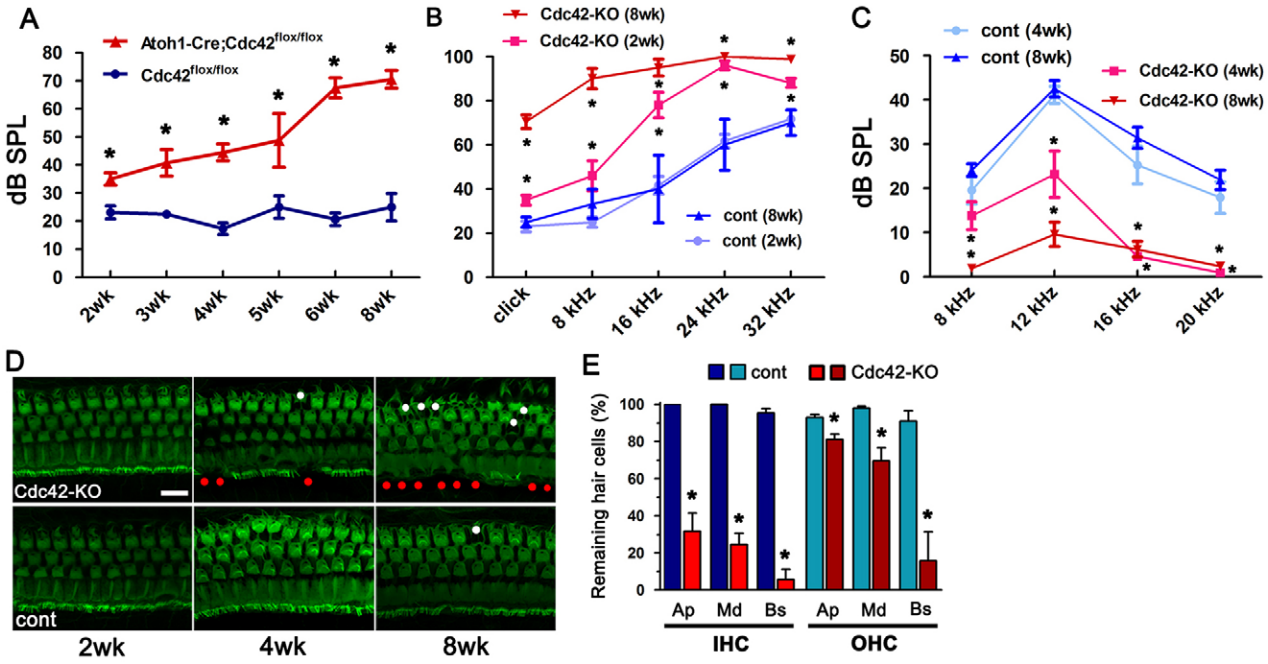

Fig. 2. Slowly progressive hearing and hair cell loss in *Atoh1–Cre;Cdc42$^{flox/flox}$* mice. (A) Age-related click ABR thresholds (dB SPL) in *Cdc42$^{flox/flox}$* (cont, blue) and *Atoh1–Cre;Cdc42$^{flox/flox}$* (Cdc42-KO, red) mice. $n \geq 4$ animals; *$P<0.05$. (B) Age-related click and tone-burst (8, 16, 24 and 32 kHz) ABR thresholds in *Cdc42$^{flox/flox}$* and *Atoh1–Cre;Cdc42$^{flox/flox}$* mice. *Atoh1–Cre;Cdc42$^{flox/flox}$* mice show a progressive and high-frequency sound-dominant hearing loss. $n \geq 4$; *$P<0.05$. (C) Age-related DPOAE (f2 frequency at 8, 12, 16 and 20 kHz) thresholds in *Cdc42$^{flox/flox}$* and *Atoh1–Cre;Cdc42$^{flox/flox}$* mice. Progressive and high-frequency sound-dominant hearing loss is detected. $n \geq 4$; *$P<0.05$. (D) Representative ($n \geq 4$) Alexa-Fluor-488–phalloidin staining shows hair cell loss (white and red circles) in the middle turn of cochleae from *Cdc42$^{flox/flox}$* and *Atoh1–Cre;Cdc42$^{flox/flox}$* mice at the age of 2, 4 and 8 weeks. (E) The percentages of remaining IHCs and OHCs in each turn in *Cdc42$^{flox/flox}$* and *Atoh1–Cre;Cdc42$^{flox/flox}$* mice at 8 weeks. Note the IHC- and basal turn (Bs)-dominant hair cell loss. $n \geq 3$; *$P<0.05$. Ap, apical; Md, middle.

epithelia [organ of Corti, vestibular macula, and crista ampularis] of *Atoh1–Cre;Cdc42$^{flox/flox}$* mice at P0 and 2 weeks (supplementary material Fig. S1C). The number of IHCs and OHCs labeled with the hair-cell-specific marker myosin VIIa in *Atoh1–Cre;Cdc42$^{flox/flox}$* mice at 2 weeks was identical to that in control mice, suggesting that the development of IHCs and OHCs was normal (data not shown). However, losses of IHCs and OHCs were occasionally detected without any changes in the spiral ganglion or stria vascularis in *Atoh1–Cre;Cdc42$^{flox/flox}$* mice at 8 weeks (supplementary material Fig. S1C); therefore, we focused on hair cell viability. Phalloidin staining of the filamentous actin (F-actin) in *Atoh1–Cre;Cdc42$^{flox/flox}$* mice indicated loss of hair cells in the middle turn of the cochlea at 4 weeks (Fig. 2D) and extensive loss at 8 weeks, particularly in IHCs and in the basal turn (Fig. 2D,E), which was consistent with reduced sensitivity to high frequencies. In contrast, the number of hair cells and the shapes of kinocilia and stereocilia in the vestibule were normal in *Atoh1–Cre;Cdc42$^{flox/flox}$* mice at 5 weeks (supplementary material Fig. S1D,E).

Localization and activation of Cdc42 at stereocilia and AJCs in cochlear hair cells

We next identified the site where Cdc42 has prominent functions in hair cells. Because precise structural features were lost in TCA-fixed immunostained samples, we expressed adenovirus-encoded GFP–Cdc42 or GFP–Cdc42(T17N;4A), an inactive Cdc42 mutant lacking the membrane-targeting motif, in organotypic cochlear explants. Intense GFP–Cdc42 fluorescence was observed in confocal reconstructions at stereociliary membranes and AJCs (Fig. 3A). In contrast, GFP–Cdc42(T17N;4A) was not localized to the stereocilia or AJCs (Fig. 3B). To investigate whether Cdc42 is active and functioning at stereociliary membranes and AJCs, we examined organs of Corti harvested from P2 transgenic mice expressing a Cdc42 fluorescence resonance energy transfer (FRET) biosensor (Cdc42-FRET biosensor mice) using two-photon excitation fluorescence microscopy (Fig. 3C). The FRET:CFP ratio (hereafter FRET/CFP) was intense at stereociliary membranes (Fig. 3D) and higher at the apical cell–cell junctions (apicolateral membranes) than that at the basolateral membranes (Fig. 3D). Intriguingly, the FRET/CFP ratio was higher in the upper portions than in the basal portions of stereocilia (Fig. 3D–F). These high FRET/CFP ratios decreased significantly following treatment with the selective Cdc42 inhibitor ML141 (Fig. 3G). Moreover, high FRET/CFP ratios at the stereocilia and AJCs were also observed at P9 when hair cells are functionally and structurally mature (Frolenkov et al., 2004) (data not shown).

Progressive degeneration and loss of cochlear hair cells in *Atoh1–Cre;Cdc42$^{flox/flox}$* mice

We analyzed the ultrastructure of organs of Corti, particularly stereocilia, in *Atoh1–Cre;Cdc42$^{flox/flox}$* mice using scanning electron microscopy (SEM). The regular arrangement of IHCs and OHCs was maintained in control mice at 8 weeks (Fig. 4A). Stereocilia in IHCs were arranged into a few gently curved rows with a moderately determined length in each row (Fig. 4G), whereas OHC stereocilia were arranged in three rows with a distinct W-shape alignment and precise length gradient among and within the rows (Fig. 4C).

The cellular arrangement and apical configuration of both IHCs and OHCs in *Atoh1–Cre;Cdc42$^{flox/flox}$* mice at P3 were

Journal of Cell Science (2014) 127, 2040–2052 doi:10.1242/jcs.143602

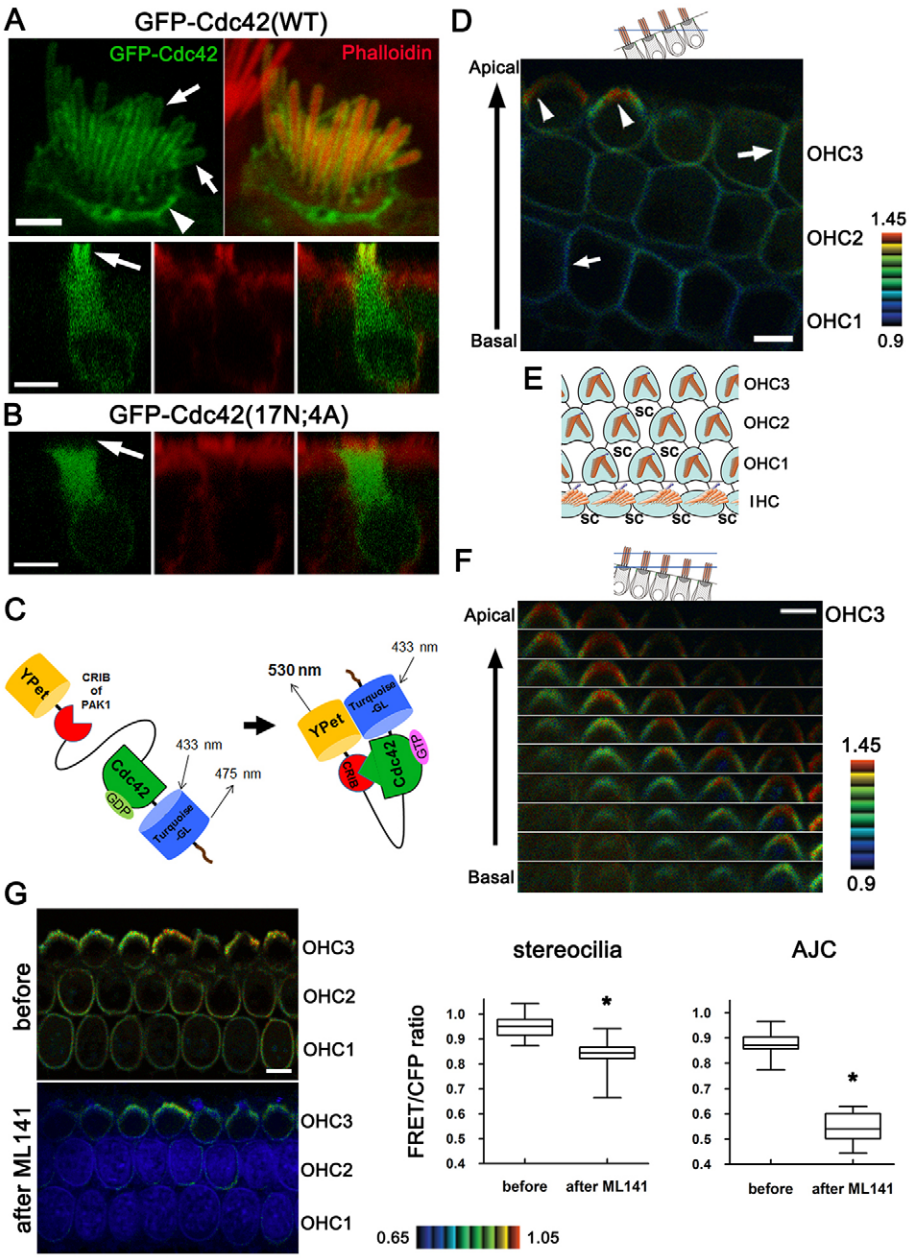

Fig. 3. Cdc42 localization and function at the hair cell stereociliary membranes and AJCs. (A,B) Dissected organ of Corti from P1 wild-type mice cultured for 16 h and infected with the indicated adenoviruses (green). The top panels of A show membrane localization of GFP–Cdc42 covering an individual stereocilum (arrows) and at apical cell junctions in a IHC (arrowhead). Scale bar: 2 μm. The lower panels of A and B show reconstructed lateral view (in the *xz* axis) images of cochlear OHCs; GFP–Cdc42, but not GFP–Cdc42(17N;4A), is localized at the stereociliary membranes (arrow). Scale bars: 10 μm (C) Schematic representation of the intramolecular Cdc42 FRET biosensor: YPet and Turquoise-GL are variants of YFP and CFP, respectively. (D–G) Dissected organ of Corti from P2 Cdc42-FRET mice were observed under a two-photon excitation microscope. D, F and G are obtained from different organs of Corti. Scale bars: 10 μm. (D) The FRET/CFP ratio is highest at the stereocilia (arrowheads) and is higher at the apicolateral membranes (large arrow) than at the basolateral membranes (small arrow). Note that the image plane is oblique to the apical surface to show cross-sections of various depths, from the level of stereocilia to that of the basolateral membrane (see the illustration above it). A 3D movie is available in supplementary material Movie 1. (E) Schematic drawing showing an overview of IHCs and OHCs1–3 in an organ of Corti. (F) Composite image showing the FRET/CFP ratio of a series of five OHCs in the row of OHC3 obtained in serial sections from the base to top of stereocilia. Note that the five OHCs are obliquely aligned in vertical direction (see the illustration). The FRET/CFP ratio is higher in upper portions than in basal portions of stereocilia in all OHCs. (G) Representative FRET/CFP ratio images ($n \geq 3$) showing the effect of the Cdc42 inhibitor ML141 (before and 4 min after 500 μM ML141 treatment). The right-hand panel shows a quantification of these results (mean ± s.e.m.) showing that FRET/CFP ratios at the stereocilia and AJCs are significantly decreased by ML141. *$P<0.01$.

identical to those in control mice (supplementary material Fig. S1F). At P8, IHCs in *Atoh1–Cre;Cdc42*$^{flox/flox}$ mice obtained a mature shape, in which kinocilia were ablated and stereocilia were aligned in rows in a staircase pattern, which was the same as control IHCs (Fig. 4E). The shape and array of stereocilia in OHCs were also indistinguishable from those in control mice (Fig. 4F). However, when hearing was fully mature at 2 weeks, occasional IHC degeneration with partial stereocilia fusion was observed in *Atoh1–Cre;Cdc42*$^{flox/flox}$ mice (Fig. 4H). IHCs showed further degeneration and were randomly eliminated at 4 weeks (Fig. 4I), and IHC loss and stereocilia fusion were frequently observed in the middle turn of the cochlea at 6 weeks (Fig. 4J). Finally, most IHCs were lost at 8 weeks, except for a small number of IHCs with fused rod-like stereocilia in the middle turn (Fig. 4B). IHCs were more frequently present in the apical turn at 8 weeks, but stereocilia were often fused (Fig. 4K–M). In the middle turn of *Atoh1–Cre;Cdc42*$^{flox/flox}$ mice, the percentage of IHCs with fused stereocilia was 15.2%, 31.4%, 42.8% and 88.2% at 2, 4, 6 and 8 weeks, respectively.

The degeneration and loss of OHCs were much less pronounced than that of IHCs during this period. OHCs were occasionally lost at 8 weeks in *Atoh1–Cre;Cdc42*$^{flox/flox}$ mice (Fig. 4B), and the remaining OHCs had scattered stereocilia bundles with a disrupted W-shaped profile; however, no stereocilia fusion was observed (Fig. 4D).

Disturbed ultrastructure of stereocilia and AJCs in *Atoh1–Cre;Cdc42*$^{flox/flox}$ mice

We used transmission electron microscopy (TEM) to further examine the structural changes in stereocilia and AJCs using IHCs in the middle turn of the cochlea at 2 and 6 weeks. No apparent changes were detected in AJCs of *Atoh1–Cre;Cdc42*$^{flox/flox}$ mice at 2 weeks (supplementary material Fig. S4A,B), whereas remarkable changes were observed in the ultrastructures of stereocilia and

Journal of Cell Science (2014) 127, 2040–2052 doi:10.1242/jcs.143602

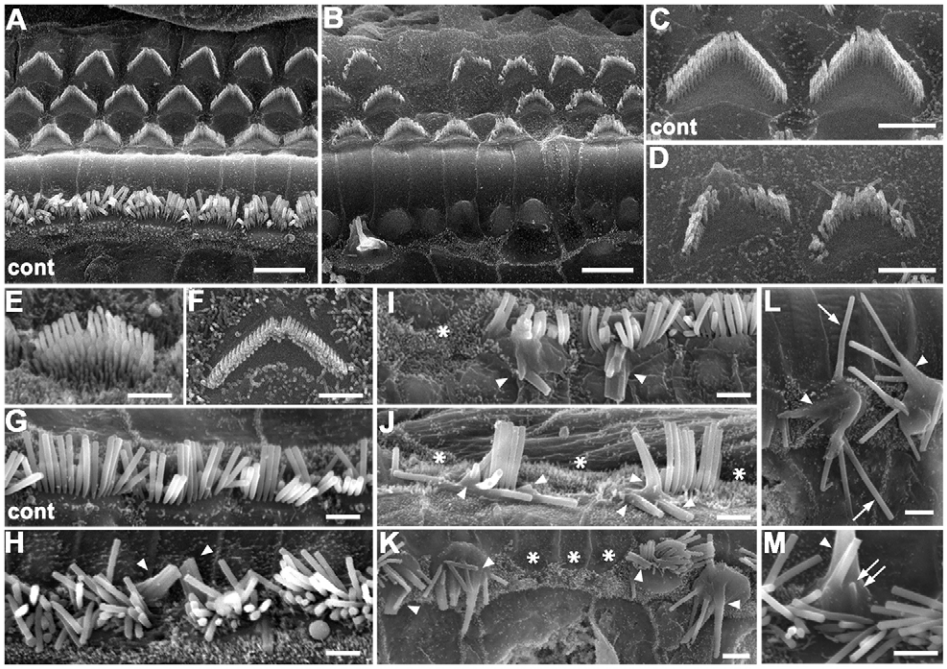

Fig. 4. Degeneration of cochlear stereocilia in *Atoh1–Cre;Cdc42*$^{flox/flox}$ mice. SEM images of the organ of Corti at the middle turn (A–J) and the apical turn (K–M) obtained from *Cdc42*$^{flox/flox}$ (cont; A,C,G) and *Atoh1–Cre;Cdc42*$^{flox/flox}$ (B,D–F,H–M) mice at the age of P8 (E,F), 2 (H), 4 (I), 6 (J), and 8 weeks (A–D,G,K–M). (A) Both IHCs and OHCs are regularly aligned in a plane in *Cdc42*$^{flox/flox}$ mice at 8 weeks. (B) In *Atoh1–Cre;Cdc42*$^{flox/flox}$ mice at 8 weeks, IHCs mostly disappeared, whereas OHCs are partially depleted and have scattered stereocilia. (C) In *Cdc42*$^{flox/flox}$ OHCs at 8 weeks, stereocilia have the characteristic W-profile. (D) In *Atoh1–Cre;Cdc42*$^{flox/flox}$ OHCs at 8 weeks, stereocilia are fewer in number and have lost their characteristic W-profile and precise staircase pattern with consistent length of stereocilia in each row. (E,F) The morphology of IHC (E) and OHC (F) in *Atoh1–Cre;Cdc42*$^{flox/flox}$ mice at P8 is identical to that in *Cdc42*$^{flox/flox}$ mice (not shown). (G) The regular array of stereocilia in IHCs of *Cdc42*$^{flox/flox}$ mice at 8 weeks. (H) In the middle turn of cochlea in *Atoh1–Cre;Cdc42*$^{flox/flox}$ mice, stereocilia fusion (arrowheads) is first observed at 2 weeks. (I–M) The stereoilia fusion (arrowheads) and IHC loss (asterisks) increase in number through 4 (I) to 6 weeks (J). The apical turn of cochlea at 8 weeks retains some IHCs, which have frequently fused stereocilia (K–M, arrowheads), and long (L, arrows) and short stereocilia (M, double arrow). Scale bars: 5 μm (A,B); 2 μm (C–L).

AJCs at 6 weeks. In contrast to the regular rows of IHCs and supporting cells (where there is a row of supporting cells adjacent to each row of IHCs) in control mice (Fig. 5A), IHCs in *Atoh1–Cre;Cdc42*$^{flox/flox}$ mice were often absent and replaced by supporting cells (Fig. 5B). IHCs in control mice were bordered by the arcuate-shaped apical junctional membrane and the underlying thick perijunctional density of the circumferential actin belt (Fig. 5A). Stereocilia in control IHCs were apically located and each had a single rootlet inserted into the cuticular plate (Fig. 5A). In contrast, the membranes at the base of stereocilia in most IHCs of *Atoh1–Cre;Cdc42*$^{flox/flox}$ mice were elevated and contained some actin cores with rootlets (Fig. 5B), which penetrated a visibly normal cuticular plate and appeared to be normal in length, indicating that these stereocilia were fused at the base. The vertical shape of AJCs was ruffled in *Atoh1–Cre;Cdc42*$^{flox/flox}$ mice compared with that in control mice (Fig. 5C). At high magnification, it could be seen that the circumferential actin belt in IHCs was thinner in *Atoh1–Cre;Cdc42*$^{flox/flox}$ mice than in control mice (Fig. 5D).

Cdc42-KD in MDCK cells as a model of Cdc42-deleted cochlear hair cells

To further confirm the effect of Cdc42 deletion and to investigate the role of Cdc42 in stereocilia and AJCs, we established an *in vitro* model using MDCK cells, which possess microvilli (structures analogous to primordial stereocilia) and have been used as a model for AJCs (Ben-Yosef et al., 2003; Nakano et al., 2009). First, we examined the subcellular localization of Cdc42 in MDCK cells stably expressing GFP–Cdc42 (MDCK$^{GFP–Cdc42}$) plated on Matrigel to produce cysts. GFP–Cdc42 fluorescence was intense at the apical membrane and weakly high at the lateral membrane of MDCK$^{GFP–Cdc42}$ cells in these cysts (Fig. 6A), consistent with a previous report (Qin et al., 2010). Next, we established MDCK cells with stable knockdown of Cdc42 (MDCK$^{Cdc42-KD}$) using the most effective shRNA plasmid sh197 (Fig. 6B,C). Using SEM, we found that the number of microvilli was significantly reduced and the cell border was often dentated at the cell junctions to partially overlie the surface of the neighboring cells in two MDCK^{Cdc42KD} clones (MDCK$^{Cdc42-KDa}$ and MDCK$^{Cdc42-KDg}$) in comparison with the control MDCK cells (MDCK^{cont}) (Fig. 6D). MDCK$^{Cdc42-KDg}$ was used for all further studies. The reduced number of microvilli and the dentated cell border in MDCK$^{Cdc42-KDg}$ cells were almost completely rescued by adenoviral-mediated expression of an shRNA-resistant form of GFP–Cdc42 but not an shRNA-resistant form of the inactive GFP–Cdc42(T17N;4A) (Fig. 6E,F). High-resolution morphological examination of MDCK$^{Cdc42-KDg}$ cells by scanning helium-ion microscopy (SHIM) showed that microvilli were scattered and had abnormally ragged, fused, short or elongated morphologies (Fig. 6G).

Finally, we examined the formation of tight junctions (TJs) in MDCK$^{Cdc42-KDg}$ cells. Although the TJ marker ZO1 was localized correctly in MDCK^{cont} cells (Fig. 7A), ZO1 was not targeted at TJs in MDCK$^{Cdc42-KDg}$ cells (Fig. 7B; similar results were obtained using MDCK$^{Cdc42-KDa}$ cells; data not shown). The localization of ZO1 at the cell junctions was recovered by

Journal of Cell Science (2014) 127, 2040–2052 doi:10.1242/jcs.143602

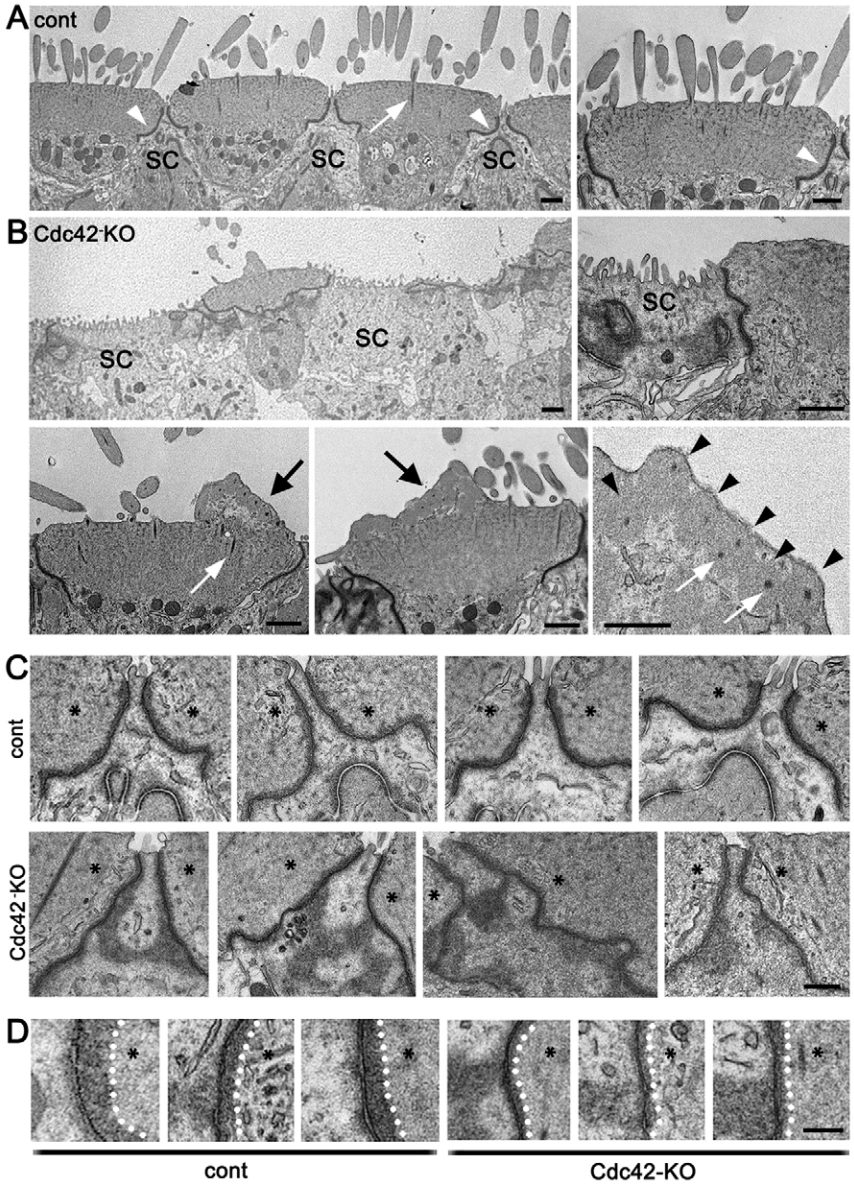

Fig. 5. Disturbed ultrastructure of stereocilia and AJCs in *Atoh1–Cre;Cdc42*$^{flox/flox}$ mice. TEM images of IHCs at the middle turn of cochlea at 6 weeks of age. (A) In *Cdc42*$^{flox/flox}$ (cont) mice, IHCs and supporting cells (SC) are alternately aligned (left) and there is a thick actin-rich cuticular plate bordered by the arcuate-shaped AJCs with the circumferential actin belt (arrowheads) observed as a dense layer beneath the plasma membrane (right, magnified view). Stereocilia are located on the apical surface and each has a single rootlet inserted into the cuticular plate (arrow). (B) Upper panels: *Atoh1–Cre;Cdc42*$^{flox/flox}$ (Cdc42-KO) mice are missing some IHCs, which were displaced by supporting cells, characterized by the apical microvilli. Lower panels: stereocilia in the remaining IHCs are often fused at the base (black arrows) and they contain several actin cores (black arrowheads) with rootlets (white arrows). The right two panels are close-up views of supporting cells with microvilli and neighboring hair cells (upper) and fused stereocilia base (lower). (C) Close-up views of the AJCs in *Cdc42*$^{flox/flox}$ (upper panels) and *Atoh1–Cre;Cdc42*$^{flox/flox}$ mice (lower panels). Each panel shows a cross section of a supporting cell in the middle, flanked by two hair cells (asterisks). The AJCs display smooth and vertical arcs in controls but shows a range of ruffling in *Atoh1–Cre;Cdc42*$^{flox/flox}$ mice. (D) Close-up views of the AJCs and perijunctional actin belts. Hair cells (asterisks) are on the right side. The actin belt (outlined by white dots) is thinner in *Atoh1–Cre;Cdc42*$^{flox/flox}$ hair cells. Scale bars: 1 μm (A,B); 500 nm (C); 200 nm (D).

introducing shRNA-resistant GFP–Cdc42 (Fig. 7C) but not GFP–Cdc42(T17N;4A) (Fig. 7D).

Altered actin-regulatory signaling in MDCK$^{Cdc42\text{-}KD}$ cells and reduced actin turnover in hair cells of *Atoh1–Cre;Cdc42*$^{flox/flox}$ mice

The disturbed ultrastructures in the stereocilia and AJCs of *Atoh1–Cre;Cdc42*$^{flox/flox}$ mice, together with the abnormalities in microvilli and TJs of MDCK$^{Cdc42\text{-}KD}$ cells, suggested that Cdc42 deletion compromises actin dynamics in stereocilia, microvilli and AJCs. To understand Cdc42 signaling in these stable actin structures, we examined several molecules associated with actin turnover in MDCK$^{Cdc42\text{-}KD}$ cells.

N-WASP, which is a downstream target of Cdc42, has a closed conformation when in the inactive state. N-WASP is activated by binding of Cdc42 to its Cdc42/Rac interactive binding (CRIB) region, together with phosphorylation at Tyr^{256} (Suetsugu et al., 2002). The phospho-N-WASP was localized at the apical surface and apicolateral membranes of MDCK^{cont}, but not MDCK$^{Cdc42\text{-}KD}$, cells plated on Matrigel (supplementary material Fig. S2A). MDCK cells with stable knockdown of N-WASP (MDCK$^{NWASP\text{-}KD}$; supplementary material Fig. S2B) plated on a filter insert had fused microvilli at their bases and a small reduction in microvilli number (supplementary material Fig. S2C,D). Furthermore, the 'wavy' staining of ZO1 in MDCK$^{NWASP\text{-}KD}$ cells indicated that TJs were abnormal (supplementary material Fig. S2E). Thus, MDCK$^{NWASP\text{-}KD}$ cells showed similar, but milder, phenotypes than did MDCK$^{Cdc42\text{-}KD}$ cells.

p21-activated kinases (PAKs) are well-known downstream targets of Cdc42, and the levels of phospho-PAK was reduced in MDCK$^{Cdc42\text{-}KD}$ cells (Fig. 8A), whereas phosphorylation of LIMK (Fig. 8A) and cofilin (Fig. 8B), which are downstream targets of PAKs, was unexpectedly increased in both clones of MDCK$^{Cdc42\text{-}KD}$ cells, consistent with a previous report (Garvalov et al., 2007). Given that LIMK is a substrate of Rho-associated protein kinases (ROCKs) (Amano et al., 2010), we examined phosphorylation of the ROCK substrate myosin phosphatase targeting subunit 1 (MYPT1) and found that it was enhanced in

Journal of Cell Science (2014) 127, 2040–2052 doi:10.1242/jcs.143602

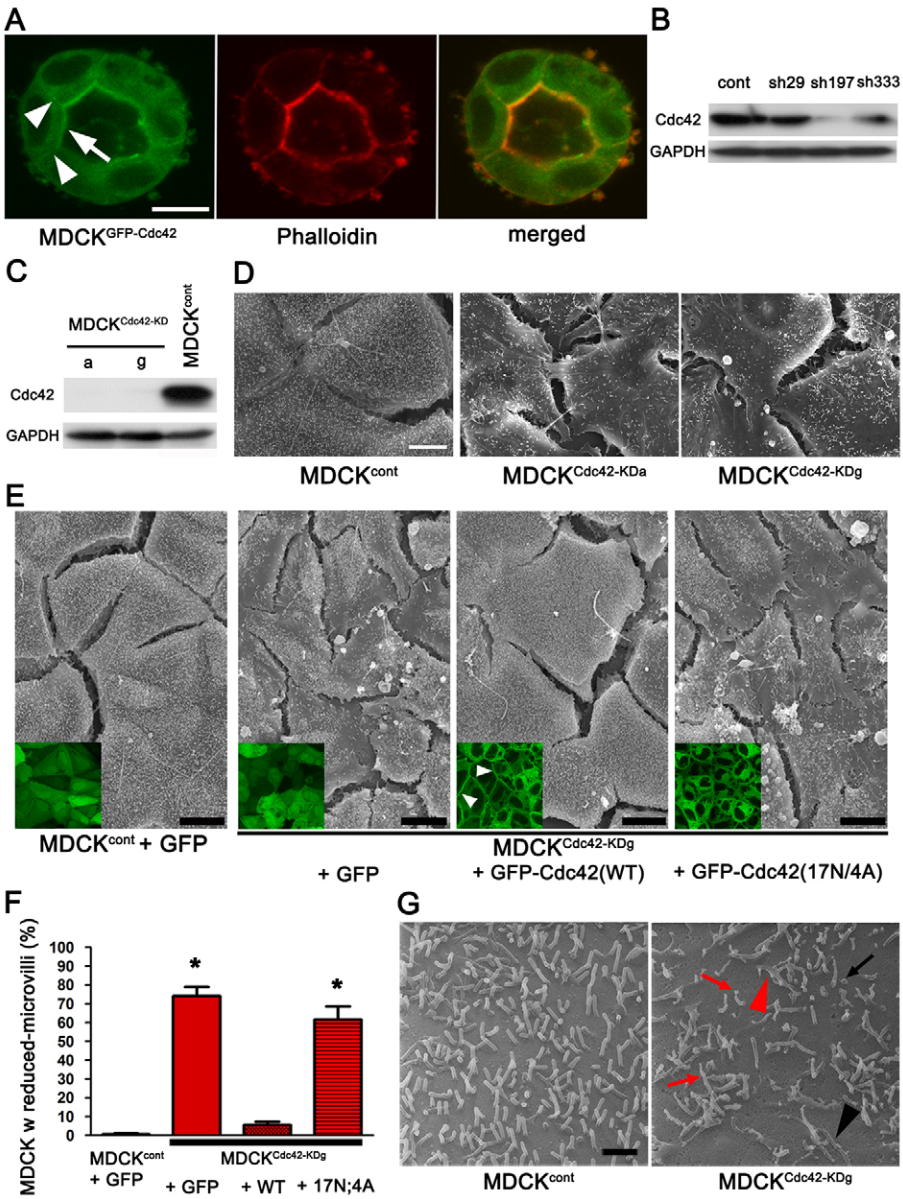

Fig. 6. Reduced number and shape-abnormalities of microvilli in MDCK$^{Cdc42\text{-}KD}$ cells. (A) Confocal images of MDCK$^{GFP\text{-}Cdc42}$ cells cultured in Matrigel and counterstained with Alexa-Fluor-568–phalloidin. Note the strong and weak GFP–Cdc42 accumulation at the apical (arrow) and lateral surfaces of cyst-cells (arrowheads), respectively. Scale bar: 10 µm. (B,C) Immunoblot showing the effects of three different shRNA-plasmids targeting canine *Cdc42* (sh29, sh197, sh333) in MDCK cells. Using the most effective shRNA (sh197), two different clones (MDCK$^{Cdc42\text{-}KDa}$ and MDCK$^{Cdc42\text{-}KDg}$) were established. (D) SEM images showing the apical surface of MDCK cells grown on a filter insert. Both MDCK$^{Cdc42\text{-}KDa}$ and MDCK$^{Cdc42\text{-}KDg}$ cell lines had substantially fewer microvilli compared with cells expressing a control shRNA (MDCK^{cont}). Scale bar: 5 µm. (E) SEM images of MDCK^{cont} and MDCK$^{Cdc42\text{-}KDg}$ cells grown on a filter insert, and infected by the indicated adenoviruses. Colored insets show the GFP signal. Note the localization of GFP–Cdc42 at cell–cell junctions (arrowheads). Scale bars: 10 µm. (F) Recovery of reduced microvilli in MDCK$^{Cdc42\text{-}KDg}$ cells by the expression of adenovirus-encoded GFP–Cdc42 but not GFP–Cdc42(17N;4A). *$P<0.01$. (G) High-power images obtained by scanning helium-ion microscope (SHIM) showing the range of morphological abnormalities in microvilli in MDCK$^{Cdc42\text{-}KDg}$ cells. Black arrow, black arrowhead, red arrows, and red arrowhead showing shortened, lengthened, ragged and fused microvilli, respectively. Scale bar: 500 nm.

MDCK$^{Cdc42\text{-}KD}$ cells (Fig. 8C). After treatment with the ROCK inhibitor Y27632, the enhanced phosphorylation of cofilin was partially normalized and that of MYPT1 was almost fully normalized (Fig. 8D). The activation of the RhoA–ROCK pathway in MDCK$^{Cdc42\text{-}KD}$ cells was confirmed using an antibody to active RhoA and an antibody to phospho-myosin light chain 2 (MLC2) (supplementary material Fig. S3A,B).

The dislocalized phospho-N-WASP and enhanced levels of phospho-cofilin suggested that Cdc42 deletion leads to reduced actin turnover in MDCK$^{Cdc42\text{-}KD}$ cells. To test whether the actin turnover was also reduced in hair cells, we evaluated the actin depolymerization rate in the hair cells of *Atoh1–Cre;Cdc42$^{flox/flox}$* mice. We added an actin polymerization inhibitor cytochalasin D, which arrests actin polymerization and causes shortening of stereocilia by continuous depolymerization at the minus ends of F-actin, to the explant culture of organ of Corti, as previously described (Rzadzinska et al., 2004). The length of stereocilia in the areas of interest (supplementary material Fig. S3D,E) was comparable between control mice (1.47±0.03–1.85±0.04 µm) and *Atoh1–Cre;Cdc42$^{flox/flox}$* mice (1.46±0.06–1.78±0.05 µm) before treatment with cytochalasin D, but was significantly reduced by treatment with cytochalasin D (supplementary material Fig. S3F). As expected, stereocilia after treatment was slightly but significantly longer in *Atoh1-Cre;Cdc42$^{flox/flox}$* mice (1.11±0.02–1.20±0.04 µm) than in control mice (0.99±0.02–1.04±0.02 µm) (supplementary material Fig. S3F), i.e. the rate of stereociliary shortening was less in *Atoh1–Cre;Cdc42$^{flox/flox}$* mice (0.35–0.58 µm/32 h) than in control mice (0.48–0.81 µm/32 h) in all the three areas observed (supplementary material Fig. S3G).

DISCUSSION

Here, we demonstrated for the first time the localization and activation of Cdc42 at the stereociliary membranes and AJCs in cochlear hair cells by the following two methods: exogenous expression of adenovirus-encoded GFP–Cdc42 in hair cells and FRET imaging of hair cells in an explant organ of Corti from Cdc42-FRET biosensor transgenic mice. This result was supported by a study that showed that the highest FRET/CFP

Journal of Cell Science (2014) 127, 2040–2052 doi:10.1242/jcs.143602

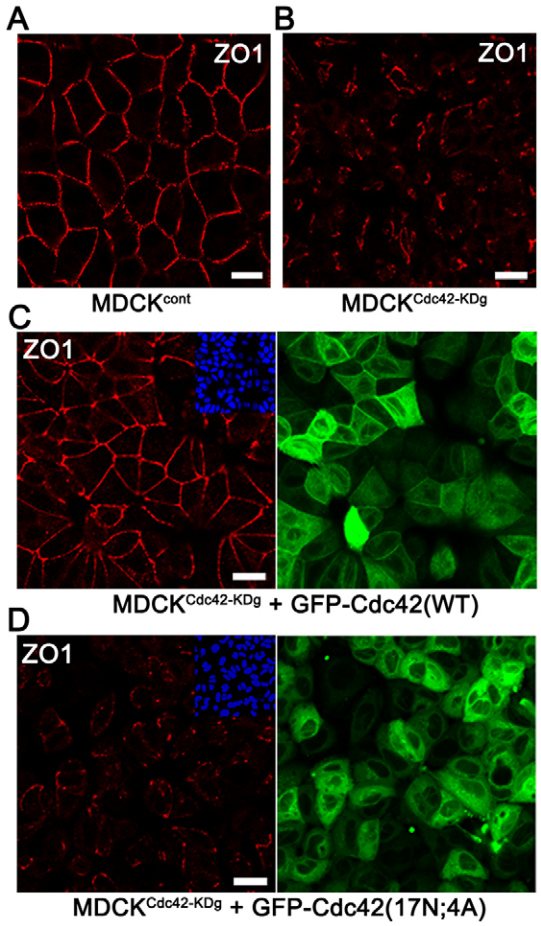

Fig. 7. Disruption of TJs in MDCK$^{Cdc42\text{-}KD}$ cells. (A,B) Confocal images of ZO1 immunostaining in confluent MDCK^{cont} (A) and MDCK$^{Cdc42\text{-}KDg}$ (B) cells. Note the absence of ZO1 at cell–cell junctions in MDCK$^{Cdc42\text{-}KDg}$ cells. (C,D) Confocal images of ZO1 immunostaining in MDCK$^{Cdc42\text{-}KDg}$ cells infected by indicated adenoviruses. Note the presence of ZO1 immunostaining at cell–cell junctions in cells expressing GFP–Cdc42 (C) but not GFP–Cdc42(17N;4A) (D). Insets, DAPI staining. Scale bars: 20 µm.

ratio of Cdc42 was at the apical surface of 3D-cultured MDCK cells (Yagi et al., 2012), thereby suggesting that Cdc42 plays a role in the microvilli. Consistent with the localization and activation profiles of Cdc42, prominent structural disturbance was observed in stereocilia and AJCs of *Atoh1–Cre;Cdc42$^{flox/flox}$* cochlear hair cells. The phenotype observed in cochlear hair cells of *Atoh1–Cre;Cdc42$^{flox/flox}$* mice might be a consequence of the direct influence of Cdc42 deletion during actin turnover in stereocilia and AJCs. This speculation was further supported by the enhanced phospho-cofilin levels in MDCK$^{Cdc42\text{-}KD}$ cells and a reduced actin depolymerization rate in the stereocilia of *Atoh1–Cre;Cdc42$^{flox/flox}$* cochlear hair cells.

The mature stereocilia in *Atoh1–Cre;Cdc42$^{flox/flox}$* mice showed a variety of degenerative changes, such as loss, shortening, fusion, and elongation. Stereocilia loss and shortening are also caused by the deletion of actin regulatory molecules located at the tip of stereocilia, e.g. espins, Eps8, myosin XVa and whirlin (Manor et al., 2011; Sekerková et al., 2011; Zampini et al., 2011). Eps8 is known to promote filopodial growth by forming the Eps8–IRSp53–Cdc42 complex (Disanza et al., 2006), and myosin XVa is the carrier protein of whirlin and Eps8 to form the myosin XVa–whirlin–Eps8 complex at the tip of stereocilia (Manor et al., 2011). The reduction of stereocilia might be partly explained by the alteration of actin polymerization and stabilization at the tip of stereocilia due to Cdc42 deficiency. Intense Cdc42 activity, particularly at the upper portions of stereocilia in Cdc42-FRET biosensor mice, also supports this possibility. However, we cannot exclude the possible involvement of a hitherto undefined or unconventional Cdc42-dependent pathway in stereocilia. Stereocilia fusion is another specific change seen in *Atoh1–Cre;Cdc42$^{flox/flox}$* mice that seemed to initiate at the base of stereocilia. Stereocilia fusion might be a consequence of the downregulation of actin depolymerization, which prevents shaping of the tapered actin core at the base and results in the 'zipping up' of the interstereociliary membrane towards the tip (Sakaguchi et al., 2008; Self et al., 1999). Alternatively, stereocilia fusion might be due to a dysfunction in the tethering of the plasma membrane to the actin cytoskeleton at the base of stereocilia. The overlapping phenotype is found in several other knockout or mutant mouse lines considered to have disturbed membrane tethering, such as those of radixin (Kitajiri et al., 2004), protein tyrosine phosphatase receptor Q (PTPRQ) (Goodyear et al., 2003) and myosin VI (Self et al., 1999). PTPRQ and myosinVI are known to cooperate at the base of stereocilia (Sakaguchi et al., 2008). However, *Atoh1–Cre;Cdc42$^{flox/flox}$* mice exhibited maintenance of specific distribution of PTPRQ and phospho-ERM proteins at the base of stereocilia (data not shown). TRIOBP-knockout mice, which maintain the stereocilia rootlet, also show fused stereocilia (Kitajiri et al., 2010); however, the rootlet structure of *Atoh1–Cre;Cdc42$^{flox/flox}$* stereocilia was unchanged (Fig. 5B). Finally, the presence of an unidentified Cdc42 function in shaping of stereocilia bases cannot be excluded.

Although Cdc42 activity in stereocilia was confirmed in both developing (P2) and mature (P9; data not shown) stages in Cdc42-FRET biosensor mice, the late-onset stereocilia phenotype observed in *Atoh1–Cre;Cdc42$^{flox/flox}$* mice suggests that the dominant involvement of Cdc42 is in the steady-state actin turnover in mature stereocilia. Late-onset progressive hearing loss associated with impaired actin turnover also occurs in *Atoh1–Cre*-mediated β- or γ-actin single knockout hair cells at 6 weeks of age, whereas deletion of both β- and γ-actin leads to stereocilia loss by P5 (Perrin et al., 2010). Thus, the common phenotype of late-onset progressive stereocilia disruption observed in β-actin or γ-actin single knockout and *Atoh1–Cre;Cdc42$^{flox/flox}$* mice suggests that a partial reduction of actin polymerization affects only the maintenance of stable actin protrusions and not their development. Alternatively, the late-onset phenotype might be explained by the compensation of Cdc42 in developing stereocilia by other actin polymerization factors, such as RhoQ, which is a small GTPase highly homologous to Cdc42 (Heasman and Ridley, 2008), and ELMOD1, which is a GTPase-activating protein of small GTPases that is temporarily expressed in hair cells during development and whose mutation results in hair cell phenotypes similar to those of *Atoh1–Cre;Cdc42$^{flox/flox}$* mice (Johnson et al., 2012).

We found increased levels of phosphorylated (inactivated) cofilin in MDCK$^{Cdc42\text{-}KD}$ cells, consistent with a study that reported that *Cdc42*-deficient neurons display increased inactivation of cofilin and arrested filopodial dynamics (Garvalov et al., 2007). Moreover, neurons lacking both the actin depolymerization factor (ADF) and cofilin (Flynn et al., 2012) exhibit reduced filopodia. These data indicate that the

Journal of Cell Science (2014) 127, 2040–2052 doi:10.1242/jcs.143602

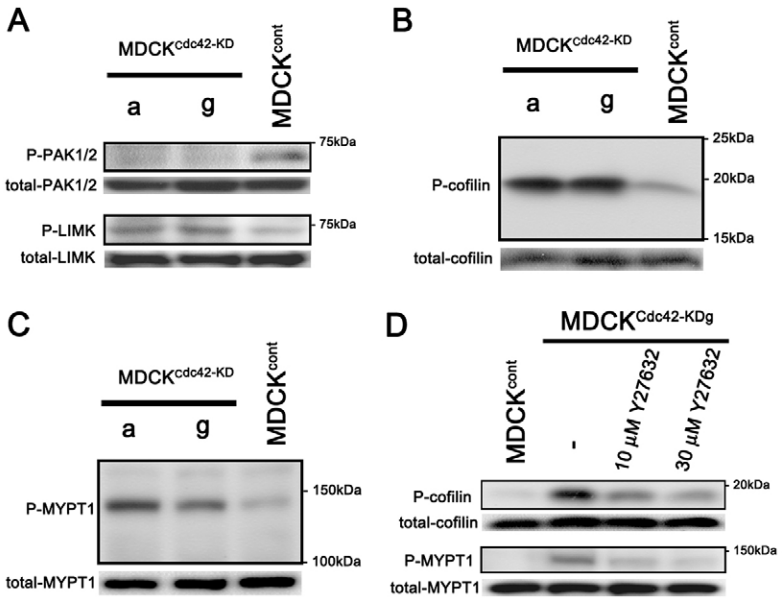

Fig. 8. Enhanced phosphorylation of cofilin and MYPT1 following Cdc42 knockdown. (A–C) Immunoblots of lysates from MDCK$^{Cdc42\text{-}KDa}$ (a), MDCK$^{Cdc42\text{-}KDg}$ (g) and MDCK^{cont} cells to detect total and phosphorylated forms of PAK1/2 and LIMK (A), cofilin (B) and MYPT1 (C). Phospho-PAK1/2 is reduced whereas phosphorylation of LIMK, cofilin and MYPT1 are all increased in MDCK$^{Cdc42\text{-}KD}$ cells. (D) Treatment of MDCK$^{Cdc42\text{-}KDg}$ cells with Y27632 at indicated concentration for 10 h moderately and almost completely inhibits the enhanced phosphorylation of cofilin and MYPT1, respectively, with dose-dependent effects.

formation and/or maintenance of actin protrusions requires the coordinated action of actin polymerization factors (e.g. Cdc42 and N-WASP) and actin depolymerization factors (e.g. ADF and cofilin), both of which are detected as stereociliary proteins (Shin et al., 2013). The balance between actin polymerization and depolymerization should be elaborately tuned in stable actin protrusions; thus, deletion of actin polymerization factors or actin depolymerization factors or both might cause downregulation of net actin turnover, which leads to structural disturbances. In fact, we confirmed the presence of a significantly, but not drastically, reduced actin depolymerization rate in the stereocilia of *Atoh1–Cre;Cdc42*$^{flox/flox}$ mice. The absence of a drastic effect might be attributed to the slow actin turnover rate in stereocilia, with the exception of the distal portion. The reduced length detected in cytochalasin-D-treated stereocilia (0.48–0.81 μm in control mice and 0.35–0.58 μm in *Atoh1–Cre;Cdc42*$^{flox/flox}$ mice) was within the range of the reported length (0.3–0.5 μm) of the distal portion of stereocilia, in which rapid actin turnover occurs (Zhang et al., 2012). Alternatively, the mild effect might be due to the limited time scale (32 h) or explant culture at P5, a time at which the morphological abnormality of hair cells had not yet appeared in *Atoh1–Cre;Cdc42*$^{flox/flox}$ mice.

Modulation of cofilin phosphorylation is complex and tightly regulated by several competitive pathways, including PAKs, LIMKs, myotonic dystrophy kinase-related Cdc42-binding protein kinase (MRCK) and ROCKs. Using MDCK$^{Cdc42\text{-}KD}$ cells, we found that Cdc42 regulates cofilin activity by antagonizing the RhoA–ROCK pathway, based on the following observations: (1) an increase of active RhoA levels (supplementary material Fig. S3A) and (2) the moderate recovery of enhanced phospho-cofilin upon treatment with Y27632 (Fig. 8D). In accordance with these results, Cdc42 suppresses RhoA signaling upstream of ROCK in brain-derived neurotrophic factor (BDNF)-stimulated neurons (Chen et al., 2006). A feedback mechanism from F-actin to RhoA for sensing the actin polymerization status might be present to control the Cdc42-mediated antagonism of RhoA signaling (supplementary material Fig. S3C). In addition, although MDCK$^{Cdc42\text{-}KD}$ cells exhibited phenotypes in microvilli similar to those of *Atoh1–Cre;Cdc42*$^{flox/flox}$ stereocilia, MDCK$^{NWASP\text{-}KD}$ cells had a less severe phenotype than those of MDCK$^{Cdc42\text{-}KD}$ cells, suggesting that there are other Cdc42-mediated actin polymerization signaling mechanisms (supplementary material Fig. S3C).

Persistent disruption of stereociliary structure and function might ultimately lead to hair cell death. For instance, deficiency of molecules with specific functions in stereocilia, e.g. PTPRQ, myosin XVa and whirlin, are known to show extensive loss of both IHCs and OHCs by the age of 12 weeks (Gong et al., 2006; Goodyear et al., 2003; Mburu et al., 2003). Stereocilia degeneration in *Atoh1–Cre;Cdc42*$^{flox/flox}$ mice began at 2 weeks when hair cell loss and AJC disruption were not observed (supplementary material Fig. S4A,B), further supporting this possibility. *Cdc42* knockdown impaired AJCs in MDCK cells, as indicated by disturbed ZO1 localization in MDCK$^{Cdc42\text{-}KD}$ cells, which is compatible with the results of previous reports (Otani et al., 2006; Popoff and Geny, 2009). The ultrastructural disturbances of AJCs in *Atoh1–Cre;Cdc42*$^{flox/flox}$ mice were observed at 6 weeks of age (Fig. 5D) but not at 2 weeks (supplementary material Fig. S4B), suggesting that Cdc42 is also involved in the long-term maintenance of the circumferential actin belt of AJCs in cochlear hair cells. The disturbance of AJCs in *Atoh1–Cre;Cdc42*$^{flox/flox}$ mice was more mild than that observed in MDCK$^{Cdc42\text{-}KD}$ cells, probably because of the heterologous (only hair-cell–supporting-cell but not hair-cell–hair-cell) cellular connection at the level of AJCs in the organ of Corti (Fig. 3E). The complex between Cdc42, PAR proteins and atypical PKC (aPKC) is a well-known polarity regulator at the apical domain of cells (Ishiuchi and Takeichi, 2011; Suzuki and Ohno, 2006). Our immunohistological analysis showed impaired apical localization of aPKC in both IHCs (supplementary material Fig. S4C–F) and OHCs (data not shown) of *Atoh1–Cre;Cdc42*$^{flox/flox}$ mice, suggesting that the Cdc42–PARs–aPKC complex might also be involved in the disturbance of apical domains in hair cells, including stereocilia roots and bases, and AJCs. Dysfunction of the epithelial barrier might affect hair cell morphology and viability in *Atoh1–Cre;Cdc42*$^{flox/flox}$ mice, similar to that previously reported in mice with mutations in the TJ proteins claudin 14 and claudin 9. However, because claudin-mutant mouse lines are severely deaf as early as P15–16 and hair cell loss is almost exclusively limited

to OHCs (Ben-Yosef et al., 2003; Nakano et al., 2009), it is unlikely that the *Cdc42*-deficient phenotypes are primarily or solely caused by dysfunction of the epithelial barrier. Finally, IHC-dominant loss is unique to *Atoh1–Cre;Cdc42*$^{flox/flox}$ mice. In general, IHCs are less vulnerable than OHCs to various etiologies such as aging, noise damage, ototoxic agents and genetic disorders (Schacht et al., 2012). A simple explanation for the predominance of the IHC phenotype is compensation by actin-regulatory molecules specific to OHCs, such as erythrocyte protein p55 (Mburu et al., 2006) and gelsolin (Mburu et al., 2010), which might be required for the maintenance of a more rigorously ordered alignment and length of stereocilia in OHCs than that in IHCs.

In summary, *Cdc42* deletion caused the downregulation of actin turnover in cochlear hair cells, which resulted in morphological abnormalities in stereocilia, with additional disturbances in AJCs after maturation, ultimately leading to slowly progressive cochlear hair cell loss. Further research is required to explore further the Cdc42 signaling(s) associated with maintenance of stereocilia (supplementary material Fig. S3C) and to verify whether abnormal ciliation is directly related to hair cell viability.

METHODS

Animals

This study was approved by the Institutional Animal Care and Use Committee and carried out according to the Kobe University Animal Experimentation Regulations. *CAG-*^{flox}*CAT*^{flox}*-LacZ* mice (Sakai and Miyazaki, 1997) and Cdc42-FRET biosensor mice (Goto et al., 2013) are as previously described. *Cdc42*^{flox} has *loxP*-sites flanking exon 2 (Aizawa et al., 2012). *Atoh1–Cre;Cdc42*$^{flox/+}$ progeny of *Cdc42*$^{flox/flox}$ and *Atoh1–Cre* (Matei et al., 2005) mice were backcrossed with *Cdc42*$^{flox/flox}$ to obtain *Atoh1–Cre*;Cdc42$^{flox/flox}$ mice, which were backcrossed to *Cdc42*$^{flox/flox}$ to generate experimental animals. Offspring were genotyped by PCR using the following primer pairs: for *Atoh1–Cre*, 5′-GCATACCTGGAAAATGCTTC-3′ and 5′-CCAGTGAAACAGCATTGCTG-3′; for *Cdc42*^{flox}, 5′-ATCGGTCACTGTTCTACTTTG-3′ and 5′-TACTGCTATGACTGAAAACCTC-3′.

Antibodies and chemicals

The following specific antibodies were used (polyclonal unless indicated): Cdc42, PAK1/2, phospho-PAK1/2(Ser192/204), LIMK, phospho-LIMK(Thr508/508), phospho-cofilin(Ser3)(77G2), cofilin(D3F9) monoclonal, MYPT1, MLC2 and phospho-MLC2 antibodies (all obtained from Cell Signaling Technology); Cdc42 monoclonal (BD Biosciences); N-WASP, phospho-MYPT1(Thr850), and Cre monoclonal (Millipore); phospho-N-WASP (Try256; ECM Biosciences); ZO1 monoclonal (1A12; Invitrogen); PKCζ (C-20, Santa Cruz); acetylated tubulin monoclonal (Sigma-Aldrich); myosin VIIa (Proteus Bioscience); GFP and GADPH monoclonal antibody (MBL International). ML141, a selective inhibitor for Cdc42 (Surviladze et al., 2010) and Y27632, a selective inhibitor of ROCK, were from MERCK and Wako Pure Chemicals, respectively. Alexa-Fluor-488 (or 568)-conjugated phalloidin and secondary antibodies were from Invitrogen.

Plasmids

Human *Cdc42* was amplified by PCR using cDNA (MTC panel II; Clontech) and cloned into *pUC118*. All mutations were introduced using QuickChange Lightning Site-Directed Mutagenesis kit (Agilent Technologies) and subcloned into pEGFP(C1). Cdc42(T17N;4A) was made by introducing a dominant-negative (T17N) and a membrane-targeting-defective [the polybasic motif (KKSRR, 183–187 aa) in Cdc42 C-terminal was changed into AASAA] mutation (Ueyama et al., 2006).

The short hairpin RNA (shRNA) expression plasmids containing a target sequence were made using pSUPER(neo) (OrigoEngine). Three target sequences for *Cdc42* knockdown (KD) tested were sh197 [canine nucleotides 197–215 from ATG, 5′-GATTACGACCGCTGAGTTA-3′, previously established (Qin et al., 2010)], sh29 (5′-GCGATGGTGCC-GTTGGTAA-3′) and sh333 (5′-GCTTGTTGGGACCCAAATTGA-3). Two target sequences for N-WASP knockdown tested were sh1396 (canine nucleotides 1396–1416, 5′-GGAATTGTGGGTGCATTAATG-3′) and sh1405 (5′-GGTGCAT TA ATGGAAGTAATG-3′). sh197-resistant GFP–Cdc42 and GFP–Cdc42(T17N;4A) plasmids were made by placing six silent changes within the targeting sequence (lowercase letters; 5′-GcTTAaGgCCatTaAGTTA-3′).

Preparation of adenovirus solutions for expression of GFP, GFP–Cdc42 and GFP–N-WASP

GFP, GFP–Cdc42 and GFP–Cdc42(T17N;4A), resistant to sh197, were amplified by PCR and cloned into the pDONR221 entry vector (Invitrogen). GFP, GFP–Cdc42 and GFP–Cdc42(T17N;4A) in the pAd/CMV/V5-DEST destination vector (Invitrogen) were obtained using the pDONR221 constructs and Gateway technology (Invitrogen). The initial adenovirus solution was made by transfection of HEK293-FT cells (Invitrogen) with PacI-digested destination plasmid using FuGENE HD (Promega). The final high-titer virus solution was obtained by CsCl buoyant density centrifugation followed by dialysis. The final titer of the virus solution was $\sim 10^{11}$ PFU/ml.

In situ hybridization

ISH was performed as described previously (Choijookhuu et al., 2012) using P5 wild-type mice. 45-base DNA antisense (coding nucleotides 432–476 in mouse Cdc42; 5′-GCAGAGCACTCCACATACTTGAC-AGCCTTCAGATCCCGCGCCAGC-3′) and sense (5′-GCTGGCGCG-GGGATCTGAAGGCTGTCAAGTATGTGGAGTGCTCTGC-3′) probes were labeled at their 5′-end with digoxigenin-11-dUTP.

X-gal and H&E stainings

X-gal staining was used to detect β-galactosidase expression in whole embryos and dissected inner ears, as previously described (Kassai et al., 2008). Samples for histology were embedded in paraffin wax and 5-µm-sections were collected on glass slides, de-paraffinized, and stained using Myer hematoxylin and Eosin (H&E) solution (Muto Pure Chemicals). X-gal and H&E stainings were photographed by using a light microscope (Axioplan II; Carl Zeiss) with a DP26 camera (Olympus).

ABR and DPOAE measurements

To assess hearing, *Atoh1–Cre;*Cdc42$^{flox/flox}$ and littermate control mice at the age of 2, 3, 4, 5, 6 and 8 weeks were tested by auditory brainstem response (ABR) measurement either unilaterally or in both ears separately. At least four animals were tested in each group, and the number of tested ears was 13, 16, 22, 6, 14, 28 for control mice and 16, 12, 31, 8, 28, 40 for *Atoh1–Cre;*Cdc42$^{flox/flox}$ mice at 2, 3, 4, 5, 6 and 8 weeks, respectively. Mice were anesthetized with 50 mg/kg of body weight pentobarbital by intraperitoneal injection and placed on a heating pad. Reference, ground and earth needle electrodes were placed subcutaneously just posterior to the subjected ear, just anterior to the other ear and at the vertex, respectively. Click or tone burst stimuli at 8, 16, 24, or 32 kHz were generated using SigGenRp software through an EC1 condenser speaker and conducted to the testing ear canal with a plastic acoustic tube. ABR recording was performed using BioSigRP software together with TDT System 3 Real-time Signal Processing Systems (Tucker–Davis Technologies, FL, USA). ABR waveforms were recorded for 12.8 ms at 40,000 Hz by using 50–5000 Hz band-pass filter settings, and ABR waveforms from 500 stimuli were averaged. Hearing thresholds (dB SPL) were defined by decreasing the sound intensity by 10 dB steps and recording the lowest sound intensity level resulting in a recognizable ABR wave pattern.

For DPOAE, measurements were tested bilaterally. The number of ears tested was 10, 8 and 10 for control, and 12, 14 and 10 for *Atoh1–Cre;*Cdc42$^{flox/flox}$ mice at the age of 2, 4 and 8 weeks, respectively. DPOAEs were measured by commercial instrumentation HearID™ Auditory Diagnostic System (Mimosa Acoustics; IL, USA) combined with CUBeDIS II v2.40 (Etymotic Research; IL, USA) software. DPOAE at frequency of 2f1–f2 were elicited using two primary tone stimuli, f1

Journal of Cell Science (2014) 127, 2040–2052 doi:10.1242/jcs.143602

and f2, with sound pressure levels of 65 and 55 dB SPL respectively, with f2/f1=1.20. A custom plastic ear tip (diameter of 3 mm) attached to an ER-10C (Mimosa Acoustics; IL, USA) probe was inserted into the ear canal and DPOAE amplitude was measured at f2 frequencies of 8, 12, 16 and 20 kHz and plotted after subtraction of noise floor amplitude.

Immunohistochemistry

Dissected tissues were fixed by 4% paraformaldehyde (PFA) in 0.1 M phosphate buffer (pH 7.4) or 10% TCA solution (Hayashi et al., 1999). After permeabilization with PBS containing 0.3% Triton X-100 (PBS-0.3T), fixed tissues were incubated with primary antibody for 2 h at 25℃ in PBS-0.03T and 0.5% fat-free BSA, followed by Alexa-Fluor-488 (or 568)-conjugated secondary antibody or phalloidin for 1 h at 25℃, and mounted in Prolong anti-fade (Invitrogen) with a coverslip. MDCK cells on the glass-bottomed dish, slide glass with Matrigel (BD Biosciences) or 0.45-µm polyester filter insert were fixed by 4% PFA in 0.1 M phosphate buffer. After permeabilization with PBS-0.3T, fixed cells were incubated with primary antibody in PBS-0.03T with 0.5% fat-free BSA, followed by Alexa-Fluor-conjugated secondary antibody, and counterstained with Alexa-Fluor-conjugated phalloidin and DAPI (Invitrogen). Immunostainings were observed under a LSM700 confocal microscope (Carl Zeiss).

Counting of IHCs and OHCs, and evaluation of vestibular hair cells

For cell counting of IHCs and OHCs from three *Cdc42*$^{flox/flox}$ and *Atoh1–Cre;*Cdc42$^{flox/flox}$ mice at 2 weeks, fixed organs of Corti were stained for myosin VIIa and with phalloidin. Three visual fields of interests were selected from the apical, middle and basal turns respectively, and the number of myosin-VIIa-positive hair cells per unit area was counted. The unit area was defined as a field including ten pillar cells, to normalize for shrinking or skewing of the sample. For evaluation of vestibular hair cells, fixed utricular maculae were stained with myosin VIIa antibody and propyl iodide. Five confocal images per hair cell layer, which was identified as the area where myosin-VIIa-positive cells mostly occupied, of each macula obtained from three *Cdc42*$^{flox/flox}$ and *Atoh1–Cre;*Cdc42$^{flox/flox}$ mice were taken, and the number of nuclei in myosin-VIIa-positive cells per image was analyzed.

SEM and TEM

Freshly dissected inner ear tissues were fixed in 2% PFA, 2.5% glutaraldehyde (GA) in 0.1 M PB. Organ of Corti epithelia were dissected in the same buffer and postfixed with 1% OsO_4 in H_2O for 2 h. For SEM, tissues were dehydrated in an ethanol series, followed by isoamyl acetate, and dried in a HCP-2 critical-point dryer (Hitachi Koki, Japan). Dried samples were mounted on stubs and examined on a Hitachi S-2380 scanning electron microscope at 10 kV. Precise visualization of MDCK microvilli was performed using an SMT ORION PLUS scanning helium-ion microscope (SHIM; Carl Zeiss), which has much higher resolution than conventional SEM (Notte et al., 2010). For TEM analysis, samples were embedded in Epon 812 resin after post-fixation (Okenshoji, Japan), polymerized at 60℃ overnight and ultra-thin sections (thickness ~70 nm) were cut on an ultramicrotome (EM-UC7; Leica Microsystems, Germany), placed on copper grids and examined on Hitachi H-7100 electron microscope at 80 kV.

Organotypic explant culture of cochlea and adenoviral infection

P2 organotypic organs of Corti explant cultures were prepared as previously described (Sakaguchi et al., 2008). For adenoviral infection, 2 µl of the high-titer adenoviral solution was added to the culture medium (*ex vivo* day 1) for 2 h. The explants were fixed 4–10 days after the infection with 4% PFA in 0.1 M phosphate buffer, counterstained with Alexa-Fluor-568-conjugated phalloidin, and observed under a confocal microscope.

Cytochalasin D experiments using organotypic explant culture of organs of Corti

The explants of P5 organs of Corti were cultured for 6 h, and then the medium was replaced with medium containing 0.02 µM cytochalasin D. The tissues were fixed after 32 h, stained with Alexa-Fluor-488-conjugated phalloidin, and observed under a confocal microscope. IHCs, which have longer stereocilia than OHCs, in the apical turns at 0–45°, 45–90° and 90–135° from the apex were used in this experiment, as hair cells in the middle or basal turns were often severely damaged. Coverslips were slightly compressed when the tissues were mounted, and only IHCs with stereocilia appropriately spread on a plane were analyzed. The length of the highest stereocilia was measured using NIH ImageJ software. In total, analysis was performed using 120–151 IHCs in ten organs of Corti (*Cdc42*$^{flox/flox}$) and 60–77 IHCs in five to six organs of Corti (*Atoh1–Cre;*Cdc42$^{flox/flox}$) for cytochalasin D treatment, and 32–33 IHCs in two organs of Corti (*Cdc42*$^{flox/flox}$) and 21–29 IHCs in two organs of Corti (*Atoh1–Cre;*Cdc42$^{flox/flox}$) without treatment.

FRET imaging

Organs of Corti from P2 Cdc42-FRET biosensor mice were dissected in Leibovitz's L-15 medium (Invitrogen), then attached on 3.5-mm Cell-Tak coated dishes (150 µg/µl; BD Biosciences), and maintained in DMEM/F-12 supplemented with 10% FBS. FRET imaging under two-photon excitation microscopy was performed as described previously (Goto et al., 2013). Samples were maintained in an incubation chamber (Tokai Hit, Japan) and imaged using a BX61WI/FV1000 upright microscope equipped with 60× water-immersion objective (LUMPlanFLN; Olympus, Japan) connected to a Mai Tai DeepSee HP Ti:sapphire Laser (Spectra Physics, Mountain View, CA). FRET/CFP images were acquired and analyzed with MetaMorph software (Universal Imaging, West Chester, PA) and Imaris Software (Bitplane AG, Switzerland), and represented by the intensity-modulated display (IMD) mode, in which eight colors from red to blue are used to represent the FRET/CFP ratio.

Cell culture

MDCK cells (RIKEN BioResource Center) were grown in EMEM supplemented with 10% FBS (GIBCO), 3% L-Gln, 0.1% nonessential amino acids (Wako) and 1 mM sodium pyruvate, in a 5% CO_2 humidified incubator at 37℃. Clonal lines were obtained by electroporation (NEPA21; NEPA GENE Co., Ltd) and G418 selection (0.5 mg/ml; Wako). MDCK$^{GFP\text{-}Cdc42}$ cells stably express GFP–Cdc42; MDCK^{cont}, MDCK$^{Cdc42\text{-}KDa}$, MDCK$^{Cdc42\text{-}KDg}$ and MDCK$^{NWASP\text{-}KD}$ lines are stable knockdown cell lines transfected with empty pSUPER(neo) or pSUPER(neo) expressing sh197 to target *Cdc42* or sh1396 (or sh1405) to target *N-WASP*.

Three-dimensional culture of MDCK cells

To produce cysts, trypsinized MDCK cells were suspended (1×10^4/ml) in culture medium containing 2% Matrigel. A suspension of 250 µl was placed on an eight-well glass slide (Lab-Tek II; NUNC) coated with 40 µl of polymerized Matrigel, and incubated for 7 days (Yagi et al., 2012). Fixed cells counterstained with Alexa-Fluor-568-conjugated phalloidin were observed under a confocal laser microscope.

To grow microvilli on the apical surface, 1×10^4 MDCK cells were grown on a 0.45-µm polyester filter insert (12-mm diameter Transwell; Coning Inc.) for 24 h. Then, 2 µl of adenovirus solution was added to the culture medium for 2 h, and cells were cultured for an additional 4 days. After fixation, samples were observed by SEM. The percentage of MDCK cells with a reduced number of microvilli was calculated using 200 cells from four independent samples.

Immunoblotting and pull-down assay

Plasmids were transfected into MDCK cells using NEPA21 electroporator. For immunoblotting, cells were lysed in homogenizing buffer (Ueyama et al., 2006) by sonication in the presence of protease inhibitor cocktail, protein phosphatase inhibitor cocktail (Nakalai tesque), and 1% Triton X-100. Total cell lysates were centrifuged at 12,000 ***g*** for 20 min at 4℃, and the supernatants were subjected to SDS-PAGE followed by immunoblotting for 2 h at 25℃ using primary antibody diluted in PBS-0.03T containing 0.5% fat-free BSA. Active RhoA was detected with the RhoA Activation Assay Kit (NewEast Biosciences)

based on pull-down assays using the monoclonal antibody specifically recognizing active RhoA. The bound primary antibodies were detected with secondary antibody conjugated to horseradish peroxidase (HRP) using the ECL detection system (GE Healthcare).

Statistical analysis

All data are presented as the mean±s.e.m. Two groups were compared using unpaired two-tailed Student's *t*-test. For comparisons of more than two groups, one-way ANOVA or two-way ANOVA was performed and followed by Bonferroni's *post hoc* test of pairwise group differences. Statistical analyses were performed using Prism 5.0 software (GraphPad); $P<0.05$ was considered statistically significant.

Competing interests

The authors declare no competing interests.

Author contributions

T.U. and N.S. planned the project. T.U., H.S., T.N., S.M., A.S. and Y.N. performed most of experiments. A.G. and M.M. performed experiments and analyzed data obtained using FRET biosensor mice. K.N., H.K., A.A. and B.F. provided the animals. Y. Hishikawa and T.K. performed ISH. H.S. and S.S. planned, performed and discussed the experiments about actin turnover. S.Y. analyzed data obtained using an electronic microscope. T.U., H.S., Y. Hisa and N.S. analyzed and interpreted data and wrote the manuscript.

Funding

This work was supported by MEXT KAKENHI on Innovative Areas 'Fluorescence Live imaging', (to N.S.); by the Takeda Science Foundation (to T.U.); and by JSPS KAKENHI [grant number 23592491 to H.S.]. Deposited in PMC for immediate release.

Supplementary material

Supplementary material available online at
http://jcs.biologists.org/lookup/suppl/doi:10.1242/jcs.143602/-/DC1

References

Aizawa, R., Yamada, A., Suzuki, D., Iimura, T., Kassai, H., Harada, T., Tsukasaki, M., Yamamoto, G., Tachikawa, T., Nakao, K. et al. (2012). Cdc42 is required for chondrogenesis and interdigital programmed cell death during limb development. *Mech. Dev.* **129**, 38-50.

Amano, M., Nakayama, M. and Kaibuchi, K. (2010). Rho-kinase/ROCK: A key regulator of the cytoskeleton and cell polarity. *Cytoskeleton (Hoboken)* **67**, 545-554.

Ben-Yosef, T., Belyantseva, I. A., Saunders, T. L., Hughes, E. D., Kawamoto, K., Van Itallie, C. M., Beyer, L. A., Halsey, K., Gardner, D. J., Wilcox, E. R. et al. (2003). Claudin 14 knockout mice, a model for autosomal recessive deafness DFNB29, are deaf due to cochlear hair cell degeneration. *Hum. Mol. Genet.* **12**, 2049-2061.

Campellone, K. G. and Welch, M. D. (2010). A nucleator arms race: cellular control of actin assembly. *Nat. Rev. Mol. Cell Biol.* **11**, 237-251.

Chen, F., Ma, L., Parrini, M. C., Mao, X., Lopez, M., Wu, C., Marks, P. W., Davidson, L., Kwiatkowski, D. J., Kirchhausen, T. et al. (2000). Cdc42 is required for PIP(2)-induced actin polymerization and early development but not for cell viability. *Curr. Biol.* **10**, 758-765.

Chen, P., Johnson, J. E., Zoghbi, H. Y. and Segil, N. (2002). The role of Math1 in inner ear development: Uncoupling the establishment of the sensory primordium from hair cell fate determination. *Development* **129**, 2495-2505.

Chen, T. J., Gehler, S., Shaw, A. E., Bamburg, J. R. and Letourneau, P. C. (2006). Cdc42 participates in the regulation of ADF/cofilin and retinal growth cone filopodia by brain derived neurotrophic factor. *J. Neurobiol.* **66**, 103-114.

Choijookhuu, N., Sato, Y., Nishino, T., Endo, D., Hishikawa, Y. and Koji, T. (2012). Estrogen-dependent regulation of sodium/hydrogen exchanger-3 (NHE3) expression via estrogen receptor β in proximal colon of pregnant mice. *Histochem. Cell Biol.* **137**, 575-587.

Collado, M. S., Burns, J. C., Hu, Z. and Corwin, J. T. (2008). Recent advances in hair cell regeneration research. *Curr. Opin. Otolaryngol. Head Neck Surg.* **16**, 465-471.

Collado, M. S., Thiede, B. R., Baker, W., Askew, C., Igbani, L. M. and Corwin, J. T. (2011). The postnatal accumulation of junctional E-cadherin is inversely correlated with the capacity for supporting cells to convert directly into sensory hair cells in mammalian balance organs. *J. Neurosci.* **31**, 11855-11866.

Disanza, A., Mantoani, S., Hertzog, M., Gerboth, S., Frittoli, E., Steffen, A., Berhoerster, K., Kreienkamp, H. J., Milanesi, F., Di Fiore, P. P. et al. (2006). Regulation of cell shape by Cdc42 is mediated by the synergic actin-bundling activity of the Eps8-IRSp53 complex. *Nat. Cell Biol.* **8**, 1337-1347.

Flynn, K. C., Hellal, F., Neukirchen, D., Jacob, S., Tahirovic, S., Dupraz, S., Stern, S., Garvalov, B. K., Gurniak, C., Shaw, A. E. et al. (2012). ADF/cofilin-mediated actin retrograde flow directs neurite formation in the developing brain. *Neuron* **76**, 1091-1107.

Frolenkov, G. I., Belyantseva, I. A., Friedman, T. B. and Griffith, A. J. (2004). Genetic insights into the morphogenesis of inner ear hair cells. *Nat. Rev. Genet.* **5**, 489-498.

Garvalov, B. K., Flynn, K. C., Neukirchen, D., Meyn, L., Teusch, N., Wu, X., Brakebusch, C., Bamburg, J. R. and Bradke, F. (2007). Cdc42 regulates cofilin during the establishment of neuronal polarity. *J. Neurosci.* **27**, 13117-13129.

Gong, T. W., Karolyi, I. J., Macdonald, J., Beyer, L., Raphael, Y., Kohrman, D. C., Camper, S. A. and Lomax, M. I. (2006). Age-related changes in cochlear gene expression in normal and shaker 2 mice. *J. Assoc. Res. Otolaryngol.* **7**, 317-328.

Goodyear, R. J., Legan, P. K., Wright, M. B., Marcotti, W., Oganesian, A., Coats, S. A., Booth, C. J., Kros, C. J., Seifert, R. A., Bowen-Pope, D. F. et al. (2003). A receptor-like inositol lipid phosphatase is required for the maturation of developing cochlear hair bundles. *J. Neurosci.* **23**, 9208-9219.

Goto, A., Sumiyama, K., Kamioka, Y., Nakasyo, E., Ito, K., Iwasaki, M., Enomoto, H. and Matsuda, M. (2013). GDNF and endothelin 3 regulate migration of enteric neural crest-derived cells via protein kinase A and Rac1. *J. Neurosci.* **33**, 4901-4912.

Hayashi, K., Yonemura, S., Matsui, T. and Tsukita, S. (1999). Immunofluorescence detection of ezrin/radixin/moesin (ERM) proteins with their carboxyl-terminal threonine phosphorylated in cultured cells and tissues. *J. Cell Sci.* **112**, 1149-1158.

Heasman, S. J. and Ridley, A. J. (2008). Mammalian Rho GTPases: new insights into their functions from in vivo studies. *Nat. Rev. Mol. Cell Biol.* **9**, 690-701.

Ishiuchi, T. and Takeichi, M. (2011). Willin and Par3 cooperatively regulate epithelial apical constriction through aPKC-mediated ROCK phosphorylation. *Nat. Cell Biol.* **13**, 860-866.

Ivanov, A. I., Hunt, D., Utech, M., Nusrat, A. and Parkos, C. A. (2005). Differential roles for actin polymerization and a myosin II motor in assembly of the epithelial apical junctional complex. *Mol. Biol. Cell* **16**, 2636-2650.

Jahan, I., Pan, N., Kersigo, J. and Fritzsch, B. (2013). Beyond generalized hair cells: molecular cues for hair cell types. *Hear. Res.* **297**, 30-41.

Johnson, K. R., Longo-Guess, C. M. and Gagnon, L. H. (2012). Mutations of the mouse ELMO domain containing 1 gene (Elmod1) link small GTPase signaling to actin cytoskeleton dynamics in hair cell stereocilia. *PLoS ONE* **7**, e36074.

Kalinec, F., Zhang, M., Urrutia, R. and Kalinec, G. (2000). Rho GTPases mediate the regulation of cochlear outer hair cell motility by acetylcholine. *J. Biol. Chem.* **275**, 28000-28005.

Kassai, H., Terashima, T., Fukaya, M., Nakao, K., Sakahara, M., Watanabe, M. and Aiba, A. (2008). Rac1 in cortical projection neurons is selectively required for midline crossing of commissural axonal formation. *Eur. J. Neurosci.* **28**, 257-267.

Kitajiri, S., Fukumoto, K., Hata, M., Sasaki, H., Katsuno, T., Nakagawa, T., Ito, J., Tsukita, S. and Tsukita, S. (2004). Radixin deficiency causes deafness associated with progressive degeneration of cochlear stereocilia. *J. Cell Biol.* **166**, 559-570.

Kitajiri, S., Sakamoto, T., Belyantseva, I. A., Goodyear, R. J., Stepanyan, R., Fujiwara, I., Bird, J. E., Riazuddin, S., Riazuddin, S., Ahmed, Z. M. et al. (2010). Actin-bundling protein TRIOBP forms resilient rootlets of hair cell stereocilia essential for hearing. *Cell* **141**, 786-798.

Manor, U., Disanza, A., Grati, M., Andrade, L., Lin, H., Di Fiore, P. P., Scita, G. and Kachar, B. (2011). Regulation of stereocilia length by myosin XVa and whirlin depends on the actin-regulatory protein Eps8. *Curr. Biol.* **21**, 167-172.

Matei, V., Pauley, S., Kaing, S., Rowitch, D., Beisel, K. W., Morris, K., Feng, F., Jones, K., Lee, J. and Fritzsch, B. (2005). Smaller inner ear sensory epithelia in Neurog 1 null mice are related to earlier hair cell cycle exit. *Dev. Dyn.* **234**, 633-650.

Matsumoto, N., Kitani, R., Maricle, A., Mueller, M. and Kalinec, F. (2010). Pivotal role of actin depolymerization in the regulation of cochlear outer hair cell motility. *Biophys. J.* **99**, 2067-2076.

Mburu, P., Mustapha, M., Varela, A., Weil, D., El-Amraoui, A., Holme, R. H., Rump, A., Hardisty, R. E., Blanchard, S., Coimbra, R. S. et al. (2003). Defects in whirlin, a PDZ domain molecule involved in stereocilia elongation, cause deafness in the whirler mouse and families with DFNB31. *Nat. Genet.* **34**, 421-428.

Mburu, P., Kikkawa, Y., Townsend, S., Romero, R., Yonekawa, H. and Brown, S. D. (2006). Whirlin complexes with p55 at the stereocilia tip during hair cell development. *Proc. Natl. Acad. Sci. USA* **103**, 10973-10978.

Mburu, P., Romero, M. R., Hilton, H., Parker, A., Townsend, S., Kikkawa, Y. and Brown, S. D. (2010). Gelsolin plays a role in the actin polymerization complex of hair cell stereocilia. *PLoS ONE* **5**, e11627.

Melendez, J., Grogg, M. and Zheng, Y. (2011). Signaling role of Cdc42 in regulating mammalian physiology. *J. Biol. Chem.* **286**, 2375-2381.

Nakano, Y., Kim, S. H., Kim, H. M., Sanneman, J. D., Zhang, Y., Smith, R. J., Marcus, D. C., Wangemann, P., Nessler, R. A. and Bánfi, B. (2009). A claudin-9-based ion permeability barrier is essential for hearing. *PLoS Genet.* **5**, e1000610.

Notte, J., IV, Hill, R., McVey, S. M., Ramachandra, R., Griffin, B. and Joy, D. (2010). Diffraction imaging in a He^+ ion beam scanning transmission microscope. *Microsc. Microanal.* **16**, 599-603.

Nunes, F. D., Lopez, L. N., Lin, H. W., Davies, C., Azevedo, R. B., Gow, A. and Kachar, B. (2006). Distinct subdomain organization and molecular composition of a tight junction with adherens junction features. *J. Cell Sci.* **119**, 4819-4827.

Otani, T., Ichii, T., Aono, S. and Takeichi, M. (2006). Cdc42 GEF Tuba regulates the junctional configuration of simple epithelial cells. *J. Cell Biol.* **175**, 135-146.
Perrin, B. J., Sonnemann, K. J. and Ervasti, J. M. (2010). β-actin and γ-actin are each dispensable for auditory hair cell development but required for Stereocilia maintenance. *PLoS Genet.* **6**, e1001158.
Ponti, A., Machacek, M., Gupton, S. L., Waterman-Storer, C. M. and Danuser, G. (2004). Two distinct actin networks drive the protrusion of migrating cells. *Science* **305**, 1782-1786.
Popoff, M. R. and Geny, B. (2009). Multifaceted role of Rho, Rac, Cdc42 and Ras in intercellular junctions, lessons from toxins. *Biochim. Biophys. Acta* **1788**, 797-812.
Qin, Y., Meisen, W. H., Hao, Y. and Macara, I. G. (2010). Tuba, a Cdc42 GEF, is required for polarized spindle orientation during epithelial cyst formation. *J. Cell Biol.* **189**, 661-669.
Rzadzinska, A. K., Schneider, M. E., Davies, C., Riordan, G. P. and Kachar, B. (2004). An actin molecular treadmill and myosins maintain stereocilia functional architecture and self-renewal. *J. Cell Biol.* **164**, 887-897.
Sakaguchi, H., Tokita, J., Naoz, M., Bowen-Pope, D., Gov, N. S. and Kachar, B. (2008). Dynamic compartmentalization of protein tyrosine phosphatase receptor Q at the proximal end of stereocilia: implication of myosin VI-based transport. *Cell Motil. Cytoskeleton* **65**, 528-538.
Sakai, K. and Miyazaki, J. (1997). A transgenic mouse line that retains Cre recombinase activity in mature oocytes irrespective of the cre transgene transmission. *Biochem. Biophys. Res. Commun.* **237**, 318-324.
Schacht, J., Talaska, A. E. and Rybak, L. P. (2012). Cisplatin and aminoglycoside antibiotics: hearing loss and its prevention. *Anat. Rec. (Hoboken)* **295**, 1837-1850.
Schwander, M., Kachar, B. and Müller, U. (2010). Review series: The cell biology of hearing. *J. Cell Biol.* **190**, 9-20.
Sekerková, G., Richter, C. P. and Bartles, J. R. (2011). Roles of the espin actin-bundling proteins in the morphogenesis and stabilization of hair cell stereocilia revealed in CBA/CaJ congenic jerker mice. *PLoS Genet.* **7**, e1002032.
Self, T., Sobe, T., Copeland, N. G., Jenkins, N. A., Avraham, K. B. and Steel, K. P. (1999). Role of myosin VI in the differentiation of cochlear hair cells. *Dev. Biol.* **214**, 331-341.
Shin, J. B., Krey, J. F., Hassan, A., Metlagel, Z., Tauscher, A. N., Pagana, J. M., Sherman, N. E., Jeffery, E. D., Spinelli, K. J., Zhao, H. et al. (2013). Molecular architecture of the chick vestibular hair bundle. *Nat. Neurosci.* **16**, 365-374.
Suetsugu, S., Hattori, M., Miki, H., Tezuka, T., Yamamoto, T., Mikoshiba, K. and Takenawa, T. (2002). Sustained activation of N-WASP through phosphorylation is essential for neurite extension. *Dev. Cell* **3**, 645-658.
Surviladze, Z., Waller, A., Strouse, J. J., Bologa, C., Ursu, O., Salas, V., Parkinson, J. F., Phillips, G. K., Romero, E., Wandinger-Ness, A. et al. (2010). A potent and selective inhibitor of Cdc42 GTPase. In *Probe Reports From the NIH Molecular Libraries Program*. Bethesda, MD: National Center for Biotechnology Information.
Suzuki, A. and Ohno, S. (2006). The PAR-aPKC system: lessons in polarity. *J. Cell Sci.* **119**, 979-987.
Takenawa, T. and Suetsugu, S. (2007). The WASP-WAVE protein network: connecting the membrane to the cytoskeleton. *Nat. Rev. Mol. Cell Biol.* **8**, 37-48.
Theriot, J. A., Mitchison, T. J., Tilney, L. G. and Portnoy, D. A. (1992). The rate of actin-based motility of intracellular Listeria monocytogenes equals the rate of actin polymerization. *Nature* **357**, 257-260.
Ueyama, T., Geiszt, M. and Leto, T. L. (2006). Involvement of Rac1 in activation of multicomponent Nox1- and Nox3-based NADPH oxidases. *Mol. Cell. Biol.* **26**, 2160-2174.
Yagi, S., Matsuda, M. and Kiyokawa, E. (2012). Suppression of Rac1 activity at the apical membrane of MDCK cells is essential for cyst structure maintenance. *EMBO Rep.* **13**, 237-243.
Yang, L., Wang, L. and Zheng, Y. (2006). Gene targeting of Cdc42 and Cdc42GAP affirms the critical involvement of Cdc42 in filopodia induction, directed migration, and proliferation in primary mouse embryonic fibroblasts. *Mol. Biol. Cell* **17**, 4675-4685.
Zampini, V., Rüttiger, L., Johnson, S. L., Franz, C., Furness, D. N., Waldhaus, J., Xiong, H., Hackney, C. M., Holley, M. C., Offenhauser, N. et al. (2011). Eps8 regulates hair bundle length and functional maturation of mammalian auditory hair cells. *PLoS Biol.* **9**, e1001048.
Zhang, D. S., Piazza, V., Perrin, B. J., Rzadzinska, A. K., Poczatek, J. C., Wang, M., Prosser, H. M., Ervasti, J. M., Corey, D. P. and Lechene, C. P. (2012). Multi-isotope imaging mass spectrometry reveals slow protein turnover in hair-cell stereocilia. *Nature* **481**, 520-524.

Journal of Cell Science